NASA TECHNICAL NOTE

NASA TN D-4492

c. 1

NASA TN D-4492

EXPERIMENTAL INVESTIGATION OF AN ACOUSTIC LINER WITH VARIABLE CAVITY DEPTH

by Bert Phillips

Lewis Research Center
Cleveland, Ohio

NATIONAL AERONAUTICS AND SPACE ADMINISTRATION • WASHINGTON, D. C. • APRIL 1968

EXPERIMENTAL INVESTIGATION OF AN ACOUSTIC LINER WITH VARIABLE CAVITY DEPTH

By Bert Phillips

Lewis Research Center
Cleveland, Ohio

NATIONAL AERONAUTICS AND SPACE ADMINISTRATION

For sale by the Clearinghouse for Federal Scientific and Technical Information
Springfield, Virginia 22151 – CFSTI price $3.00

CONTENTS

EXPERIMENTAL INVESTIGATION OF AN ACOUSTIC LINER WITH VARIABLE CAVITY DEPTH

by Bert Phillips

Lewis Research Center

SUMMARY

An acoustic liner with individually isolated resonators and variable cavity depths was tested with a nominal 20 000-pound (88.8-kN) thrust hydrogen-oxygen rocket engine. The liner damping was evaluated by comparing values of hydrogen-inlet temperature at transition into combustion instability. Three concentric tube injectors were studied. Test variables were liner cavity depth, number of liner rows, and axial position of the liner rows. Cavity gas temperature and composition were measured at the screech transition point.

A flow-induced frequency shift using a theoretical axial gas velocity profile changed the calculated resonant frequency to a value matching the pretransition noise frequency. The amplitude of the pretransition noise oscillations associated with the three injectors affected liner damping. The most effective axial position of the resonators was determined to be closest to the injector. Effectiveness of row combinations of the resonators at some other positions was also determined. There was a much higher concentration of hydrogen and hence higher sonic velocity in the resonator cavities than had been predicted in previous reports.

INTRODUCTION

The use of acoustic liners to suppress combustion instability in rocket motors has been studied at the Lewis Research Center (refs. 1 and 2). A requirement for the rigorous design of acoustic liners is a knowledge of the cavity gas properties and the effective gas velocity past the liner apertures. During the previous studies, the cavity gas properties had been obtained by extrapolating theoretical properties of the combustor gases (ref. 3) to the measured cavity temperature and pressure. Also, the effective gas velocity had been estimated by a trial and error method that best matched the experimental and theoretical results, but the value obtained did not correspond to the combustor gas velocity based on engine contraction ratio. Some effort has been made to measure a boundary-layer velocity in a rocket engine directly (ref. 4), but it is not clear that such a velocity can be used for liner design, because the only available design calculations are based on a mean chamber velocity (ref. 1).

The effect of liner length (number of rows) was evaluated in reference 1, but the effects of liner length and liner position were not separated. In addition, there is no information in the literature regarding the liner damping required to provide stability with injectors of inherently different stability characteristics. Accordingly, the purpose of the present investigation was (1) to determine cavity gas properties more accurately, (2) to determine a more realistic effective gas velocity, (3) to separate the effects of liner length and liner position relative to the injector, (4) to determine the effects of injectors with different stability characteristics on liner damping.

The effects of changes in liner configuration were evaluated by decreasing the hydrogen-injection temperature until combustion instability occurred, then comparing the values of hydrogen temperature at the transition point. The configuration with the lowest transition temperature was considered to be most stable. This rating method and the temperature ramping technique are introduced in reference 5.

In reference 1, it was demonstrated that a decrease in hydrogen-injection temperature at transition corresponded to an increase in theoretical acoustic absorption coefficient of the liner configurations under study. The implication is that decreasing the temperature increased the driving or unstable tendencies of the combustor. Therefore, in order to maintain stability at a lower temperature, the liner acoustic damping must have been correspondingly higher. If the acoustic liner is to be effective, it must increase the damping of those disturbances which cause instability rather than the instability itself. Consequently, the experimental parameters that characterize the liner performance must be measured just before instability occurs.

The gas composition was determined by sampling the cavity gas and analyzing it with a mass spectrometer. The effective gas velocity was determined by solving for the velocity required to shift the calculated resonant frequency of the liner by a predetermined amount. The effects of liner length and position were separated by testing partial-length liners at different distances from the injector.

The investigation reported herein was conducted at the Rocket Engine Test Facility using a liquid-hydrogen - liquid-oxygen rocket engine. The engine had an inner diameter of $10\frac{3}{4}$ inches (27.3 cm) and was operated at the nominal values of 300-psia (2.065-MN/m^2) chamber pressure, 20 000 pounds (88.8 kN) sea level thrust, and 95 percent characteristic exhaust-velocity efficiency.

APPARATUS

Facility

The Rocket Engine Test Facility of the Lewis Research Center is a 50 000-pound (222-kN) thrust sea level test stand equipped with an exhaust gas scrubber and muffler. The facility utilized a pressurized propellant system to deliver the propellants to the engine from the storage tanks. The facility was operated from a control room located 2000 feet (610 m) from the facility. A more complete description of the facility is given in reference 5.

Hydrogen Temperature Controller

The hydrogen-injection temperature was controlled by varying the ratio of liquid- to ambient-temperature gaseous hydrogen entering the injector. The system could reduce the inlet temperature (measured within the injector) by as much as 40° R (22.2° K) per second. The temperature ramps were automatically controlled.

Engine

The heat-sink engine used in the investigation had a 20 000-pound (88.8 kN) nominal sea level thrust. The combustion-chamber inner diameter was 10.78 inches (27.6 cm), the contraction ratio was 1.89, the length of the cylindrical portion of the combustor was 14 inches (35.6 cm), the distance from the injector to the throat was 18 inches (45.7 cm), and the nozzle expansion ratio was 1.3. The engine was operated at nominal values of 300 psia (2.065 MN/m^2) chamber pressure within a mixture ratio range of 4 to 6.

Three injectors were used in this study. The liner configurations evaluated with each are given in table I. Injector I was a 487-element concentric-tube injector with a concave faceplate; the radius of curvature of the faceplate was 20 inches (50.8 cm). The hydrogen-oxygen injection area ratio was 4.67. A faceplate view of injector I is shown in figure 1(a).

Injector IIa was a 421-element concentric-tube injector with a flat faceplate. The hydrogen-oxygen injection area ratio was 5.163. A faceplate view of injector IIa is shown in figure 1(b).

Injector IIb was very similar to injector IIa. Because of slight variations in construction, it was more prone to instability; however, its performance was equivalent to either injector IIa or I. None of the injectors tested had film cooling orifices.

Liner

The liner was fabricated from mild steel with the hot-gas side coated with zirconium oxide to reduce heat transfer. A photograph of the assembled jacket and liner is shown in figure 2. The construction allowed the cavity depths of the 272 resonators to be varied individually as desired. A sketch of the liner and jacket, with the significant dimensions, is shown in figure 3(a). To vary the cavity volume from one run to the next, it was necessary to remove an external pressure seal, thread the cavity plug to a new position, and replace the pressure seal. A detailed sketch of an individual cavity is given in figure 3(b). The liner configurations tested are given in table I.

Cavity Gas Temperature and Sampling Instrumentation

Liner cavity gas temperatures in selected resonators were measured with open-ball Chromel-Alumel thermocouples. Shown in figure 4(a) is a cavity modified to allow temperature measurement. The thermocouple was placed in the center of the cavity for all cavity depths tested.

Presented in figure 4(b) is a cavity modified for gas sampling. The 1/8-inch (0.32-cm) tubing was connected to a 500-cubic-centimeter gas bottle (pre-evacuated) with an automatically controlled valve in the line. Following the test, the samples were analyzed by the use of a mass spectrometer.

Engine Instrumentation

Instrumentation for measuring engine parameters is discussed in reference 5. The three high-frequency transducers used in the present experiment were flush mounted to the inside of the liner. The location of the transducers is shown in figure 8 of reference 5. The transducers had a nominal resonant frequency of 20 000 hertz with a frequency response that was flat to about 6000 hertz as installed.

Analysis of the high-frequency data was by a continuous-band heterodyne analyzer. Spectral analyses were obtained every 0.05 second in the range 20 to 10 000 hertz for the entire run. Because of the nature of the analyzer, spurious Fourier harmonics were frequently obtained. The only means of detecting these was by determining whether the suspected harmonics were integral multiples of the frequency of a higher amplitude signal. When it was impossible to separate the Fourier harmonics from the chamber acoustics, the spectral analyses were discarded.

PROCEDURE

The initial test procedure was to determine the hydrogen-temperature stability limit of each of the injectors without a liner over a mixture ratio range of 4 to 6. This gave the baseline for determining the subsequent improvement in stability due to each liner configuration. The general procedure for stability rating a liner was then to select an initial hydrogen-inlet temperature corresponding to the screech transition temperature for the injector without a liner. The liner evaluation tests were then run in the same manner as the baseline tests without a liner. Steady-state operation (full chamber pressure) generally occurred about 0.5 second after ignition. At this time, the hydrogen temperature was decreased until screech occurred. To prevent damage to the heat-sink hardware, the entire run duration was restricted to 3 seconds. A typical screech transition is shown in figure 5.

For gas sampling runs, the sample bottle was evacuated and then filled with helium to 5 psia (34.400 kN/m^2). The hydrogen-injection temperature was preset at a value 10 to 15 R^o (5.55 to 8.35 K^o) above the previously determined transition temperature for the given liner configuration. After steady-state operation was achieved, the temperature of the hydrogen was held as constant as possible. This was done to ensure that the gas sample would be taken under conditions that were as close as possible to the previous transition point with stable combustion. At some point after steady-state operation was achieved, an automatically timed valve opened. The pressure in the resonator cavities was at approximately 300 psia (2.065 MN/m^2), and the sample bottle pressure was at 5 psia (34.400 N/m^2). The resulting pressure differential (ΔP) forced gas from the resonator into the bottle. After a preset time interval, generally 0.5 to 1 second, the valve closed. If, at any time during the sampling period, there was any full-scale instability, the sample was discarded.

Baseline Injector Stability

The injectors used in this study were rated according to their hydrogen-injection temperatures at transition (HTT). The results of this rating are presented in figure 6. Each data point represents a full-scale instability or screech transition point in a run. The region below each transition point represents unstable operation, while the region above represents stable operation for that specific run. The screech transition temperature will be referred to hereinafter as the HTT.

Injector IIa was originally tested to determine the effect of injector type on liner damping. The results, however, indicate that injectors I and IIa have the same HTT stability. Later results, however, do show some other differences resulting from the use of the two injectors.

Injector IIb was used primarily for gas sampling experiments. Because of supposedly identical construction, it was anticipated that IIa and IIb would have the same HTT stability. The results (fig. 6) indicate that injector IIb was considerably less stable than IIa. This could have been due to small but significant variations in construction. Hardware damage due to extensive testing prevented the use of either I or IIa for gas sampling tests.

Determination of Design Frequency of Baseline Configurations

In the Introduction, it was mentioned that the liner, if it is to be effective in lowering the HTT, must be designed to absorb or suppress the disturbances that trigger instability. To determine the frequency or frequencies of oscillations that a liner must suppress (i. e., the design frequency), spectral analyses were made of the high-frequency transducer output for the baseline configurations.

Presented in figure 7 are two amplitude spectral density plots of the output of a high-frequency transducer mounted flush with the inside wall of the chamber during the same run. The difference between the plots is the time within the run. Figure 7(a) corresponds approximately to the spectrum 1/10 second before screech occurred. It is this amplitude which should be used in any liner design calculation, whereas the amplitude used in reference 1 was considerably higher and may have led to some error in calculating the absorption coefficients. The presence of discrete frequencies before instability can be noted. Figure 7(b) corresponds to a later time when the full-scale instability was achieved. The oscillations remained at approximately constant amplitude until shutdown. A large difference in the amplitudes can be noticed between figures 7(a) and (b) as well as a difference in the pretransition and post-transition frequencies.

From these and similar results for the other two injectors, a series of plots of (predominant) pretransition and post-transition frequencies can be obtained. These are presented in figure 8. The plots show a maximum amplitude for each frequency in the period 0. 4 second before transition and in the fully unstable period. These periods are termined pretransition and unstable. The acoustic mode associated with the 3000- to 3500-hertz frequency range is the first-tangential mode and that associated with the 5000- to 6000-hertz frequency range is the second-tangential mode or some combined tangential-longitudinal mode.

Figure 8(a), for injector I, shows a predominant unstable frequency of 5500 hertz. The pretransition frequencies, however, are at 5000 and 6600 hertz. Figure 8(b), for injector IIa, shows a predominant unstable frequency of between 3000 and 4000 hertz (first-tangential mode) with almost no discernible pretransition oscillations. Figure 8(c), for injector IIb, has a predominantly unstable frequency of 3400 hertz with pretransitional frequencies at 5000 and 6600 hertz. Consequently, only in the case of injectors I and IIb (figs. 8(a) and (c)), can pretransition frequencies (5000 and 6600 Hz) be specified with any confidence.

The liner should be designed for either 5000 or 6600 hertz, or perhaps both, to obtain maximum damping with injector I. It can also be noted that injectors I and IIa, with the same HTT stability, have different pretransition noise spectra.

Determination of Tuning Curve for Injector I with 8-Row Liner

The primary objective in designing an acoustic liner is to match the liner resonant frequency to the frequency of the wave which is to be damped. In figure 21 of reference 6, it was demonstrated that a Helmholtz resonator exhibits maximum damping when the resonator cavity depth is adjusted so that the resonant frequency matches the frequency of the incident wave. This is a tuning process, and a curve of absorption or damping as a function of resonant frequency or cavity depth is termed a tuning curve.

When the cavity depth of a resonator is varied and the damping curve has a maximum, the cavity depth corresponding to maximum damping is termed the tuning point or tuned depth. Referring to equation (1) of the appendix, the resonant frequency is a function of cavity liner dimensions, cavity gas sonic velocity, and the effect of gas velocity past the apertures. Conversely, when the liner cavity dimensions are defined by the tuned point and the gas sonic velocity is defined, the gas velocity effect can be determined from the tuned frequency.

The experimental transition temperatures for the full-length (8 rows) liner plotted as a function of oxidant-fuel (or mixture) ratio for a variety of resonator cavity depths (all cavities the same) are shown in figure 9. For purposes of clarity, the individual transition points were deleted and only the resulting lines are shown. A cross plot of the data in figure 9 at a mixture ratio of 5 is shown in figure 10. Instead of transition temperature, the ordinate is the difference between the baseline injector transition temperature and the transition temperature associated with the cavity depth which is called the hydrogen temperature margin.

When it is recalled that the decrease in transition temperature can be associated with an increase in acoustic damping, figure 10 can be viewed as a plot of the liner damping as a function of cavity depth. The point of maximum HTT margin corresponds to the point of maximum damping (tuned point). The tuned liner lowered the transition point by 67° R (37.2° K) with no effort made to separately tune each row. If the rows were separately tuned, complete suppression of instability down to the facility temperature limit of 60° R (33.3° K) would probably have resulted. For the configuration illustrated, optimum tuning occurred at a cavity depth of about 1.8 inches (4.57 cm); however, the shape of the curve is such that small variations from optimum tuning were not critical.

Cavity-Gas Temperatures

The cavity-gas sonic velocity c is a function of the gas composition and temperature as shown by equation (3) (see the appendix). In order to define the cavity-gas temperature at the transition point, each configuration was tested with thermocouples in selected cavities. The number of thermocouples in each configuration is given in table I. It was not possible to completely instrument the $\frac{13}{16}$-inch (2.07-cm) and $1\frac{13}{16}$-inch (4.61-cm) cavity depth configurations.

A sample of a typical temperature measured in a resonator cavity is plotted as a function of run time in figure 11. For comparison, the hydrogen-inlet temperature is plotted on the same scale. The initial peak in temperature corresponds to the point at which the chamber pressure has climbed to its steady-state value, forcing hot combustion gases into the cavity. It can be noted that the maximum temperature recorded at this point is still far below the steady-state combustion temperature of 5000° R (2780° K) which is associated with a mixture ratio of 5 and a chamber pressure of 300 psi (2.065 MN/m^2). It may be inferred that the gases forced into the cavity are combustion products mixed with cold excess hydrogen or with the cooler gases of the boundary layer within the combustion chamber.

Following this maximum at about 0.8 second after the start of the run, the temperature dropped rapidly until the transition point was reached, whereupon it increased sharply. The hydrogen-injection temperature also dropped within this same period, and the decrease in cavity gas temperature may be due to a combination of conductive losses to the liner jacket as well as unburned hydrogen flowing in the boundary layer and into the cavity. The values of the liner cavity gas temperatures at transition for configurations tested with injector I are given in table II.

Figure 12 is a cross plot of the liner cavity gas temperatures (at the transition point for all resonator configurations tested with injector I) as a function of axial position in the chamber at a mixture ratio of 5. The row number approximates the axial distance in inches (or cm). Cavity temperature was not a strong function of cavity depth. The temperature climbs to a value of approximately 800° R (444° K) at 4 inches (10.16 cm) from the injector and remains constant thereafter. Data from reference 1 are shown in figure 13 as a plot of cavity temperature at transition as a function of the open-area ratio of the liner. The temperatures were measured at a point between 4 and 5 inches (10.16 and 12.70 cm) downstream of the injector. These results are for a similar injector and a liner with the same thickness and aperture diameter reported herein. A critical difference between the liner used in reference 1 and the liner in the present tests is the lack of circumferential and axial partitions in reference 1 tests. This lack allowed internal flow and recirculation of the gases behind the liner, which would change the axial and circumferential temperature profiles and prevent rigorous comparison of the temperature profiles of reference 1 with this report. A portion of the results are superimposed on figure 12, and show surprisingly good agreement.

The ratio of aperture area to hot-gas side area σ_e for the variable cavity-depth liner of the present experiment is 0.05, and the ratio of aperture area to internal cross-sectional area of the resonator cavity σ_i is approximately 0.12 (see fig. 1(b)). The liners evaluated in reference 1 were of the array type with σ_i the same as σ_e ($\sigma_i = \sigma_e =$ 0.10). The agreement between the results of reference 1 and figure 12 suggests that when the effects of crossflow and recirculation that characterize the liner of reference 1 are neglected, the internal open area ratio σ_i is the parameter that controls the cavity temperature.

Shown in figure 14 is the variation of cavity gas temperature with time during a gas sampling run with injector IIb. The thermocouples are in the same row as the gas sampling but in different circumferential positions. The time during which the valve connecting the sampling bottle to the cavity was open is also shown in figure 14 as the sampling time. Although an effort was made to keep the chamber and cavity conditions constant, this proved to be experimentally impossible, and the cavity gas temperature dropped approximately 500° R (278° K) during the sampling time. Consequently, the sample composition was characterized by a temperature averaged over the sample time.

Cavity Gas Composition Determination

The mass spectrometer analyses during tests with injector IIb revealed that only two gases were present: water vapor and hydrogen. This was expected, because the products of combustion of hydrogen-oxygen reaction at a mixture ratio of 5 are also water vapor and hydrogen. There are some complications, however, that enter into the gas sampling experiment. The first complication arises from the volume of the gas sampling bottle. Neglecting the volume due to the line, the gas sampling bottle had a volume of 500 cubic centimeters, whereas the cavity volume was approximately 20 cubic centimeters. The gas bottle pressure was generally 200 psia (1.38 MN/m^2) after sampling; the high gas bottle pressure was necessary in order to analyze for water vapor. The cavity pressure was nominally 300 psia (2.005 MN/m^2). The resulting combination of volumes and pressures indicates that the volume of the sample in the gas bottle, as taken, was approximately 7 times the volume of the resonator cavity. The result is that there can only be speculation as to how representative the sample is of the true cavity composition.

If the bulk of the gas sample came from the region of the resonator aperture, that is, the combustor boundary layer, and if the cavity gas is similar in composition to the boundary layer, as is indicated in reference 6, then the sample would have been representative of the cavity composition. Another complication is that the temperature measured in adjacent cavities was decreasing during the sampling period (fig. 14). An average temperature was used to characterize the gas, but it is not clear that this was the best number to use. A final complication is that the mixture ratio distribution would be expected to vary both circumferentially and axially and that this variation would appear in the cavity gas composition. There was, however, only one port sampled at one axial and circumferential position (third row).

In view of these uncertainties, it was deemed necessary to compare experimental results with some theoretical model. Both theoretical and experimental gas compositions are shown in figure 15. The horizontal line of figure 15, with a water-vapor mole fraction of 0.6, is taken from reference 3 which assumed complete combustion and a mixture ratio of 5. As the gases are cooled, at some temperature the water vapor will start to condense. For a pressure of 300 psia (2.065 MN/m^2), this dewpoint is 833° R (463° K). With continued cooling, more of the water vapor will condense. The maximum mole fraction of water vapor at any given temperature is equivalent to the partial pressure at the temperature. Therefore, the portion of the curve termed the condensation region is actually the variation in water-vapor partial pressure with temperature.

The experimental and theoretical results widely disagree for cavity temperatures over 600° R (333° K). For comparison, the extrapolation used in reference 1 is also shown. Without any other information, it was decided to use the experimental results of the present experiment to predict compositions based on measured cavity temperature as a more realistic approach than that of reference 1.

Using the experimental results shown in figure 15, as well as equations from the appendix, the cavity-gas average molecular weight and sonic velocity as a function of cavity temperature at transition can be calculated. Figure 16 is a plot of the theoretical sonic velocities based on both the extrapolation used in reference 1 and on the experimentally measured values of the water vapor concentration used in this report. The difference between the two curves would result in a factor of 2 error in a calculation of the cavity resonant frequency or a factor of 5 to 10 error in a calculation of the acoustic absorption coefficient or the acoustic admittance.

The wide disagreement between theory and experiment and the complications associated with any gas sampling technique clearly indicate the desirability of having a gas of known composition in the resonator cavities. For rocket-engine acoustic liners with an array construction, such as was tested in reference 1, a hydrogen or helium gas bleed into the cavity would be one method for controlling the gas composition and temperature, thereby ensuring a knowledge of the cavity gas properties.

Shifting of Cavity Resonant Frequency

The first frequency shift effects to be discussed concern an eight-row liner with injector I. Presented in figure 17 is a plot of the variation in theoretically calculated cavity resonant frequency with row number or axial distance from the injector for a liner with a cavity depth of $1\frac{13}{16}$ inch (4.61 cm). The calculations are based on the experimental temperature data given in figure 12 and on the experimental sonic velocity results of figure 16. The spread in frequency is due to the variation in cavity temperature at the transition point as shown in figure 12. The results plotted in this figure are also tabulated in table II. The cavity depth of $1\frac{13}{16}$ inch (4.61 cm) corresponded to the tuned point (i.e., maximum reduction in HTT) as was determined by the tuning curve (fig. 10) for the entire array considered as a unit. In order to simplify the following discussions, an average frequency of 4000±500 hertz was chosen to represent all eight rows for the tuned cavity depth.

Figure 18 is a plot of the HTT reduction for the eight-row liner with injector I plotted as a function of the calculated resonant frequency f_o. The HTT reduction for each of the cavity depths tested is plotted as a function of the spread in the corresponding values of calculated cavity resonant frequency. The variation in calculated cavity resonant frequency f_o for each cavity depth l was obtained in the same manner as was demonstrated in figure 17. The resulting curve is a tuning curve with a maximum value of 48^o R (26.7^o K). Based on the arguments presented previously in this report in the section on design frequency, this tuned point should correspond to one of the two pretransition frequencies, 5000 or 6600 hertz, which are shown as dashed lines in figure 18. Clearly, some frequency shift is required to shift the tuning curve maximum from 4000 hertz to either 5000 or 6000 hertz. The following experiment was intended to determine which of the two frequencies was the design frequency for injector I.

A partial length liner with only the first row of holes was stability rated with injector I. Based on previously presented arguments, the liner configuration having a resonant frequency f_o closest to the design frequency will absorb best or provide the maximum HTT reduction. The test variables were mixture ratio and cavity depth, and the results of the test are presented in figure 19. The cavity gas temperatures at transition for the three cavity depths at a mixture ratio of 5 as well as the theoretically calculated values of resonant frequency are tabulated in table II. Presented in figure 20 is a plot of the HTT reduction as a function of f_o for the first row configuration. The cavity depth of the liner with the maximum absorption was 9/16 inch (1.43 cm) with a corresponding value of f_o equal to 7200 hertz. Because 7200 hertz is closer to 6600 than to 5000 hertz, the appropriate design frequency for injector I is 6600 hertz.

The question remains as to whether the first row is subject to a frequency shift due to the effects of flow velocity past the resonator apertures. As will be shown, the only physically possible frequency shift is an increase in the value of f_o. This would shift the resonant frequency of the 9/16-inch (1.43-cm) cavity depth liner to a value even higher than 7200 hertz and further from the highest pretransition frequency of 6600 hertz. By this reasoning, there is no frequency shift for the first row, placing a restriction on the frequency shifting mechanism.

With the appropriate design frequency known, the frequency shift (necessary for tuning) for the eight-row configuration previously discussed is from 4000 to 6600 hertz (see fig. 18). The frequency shift ratio (the shifted to unshifted frequency) is 1.65. It now remains to decide what frequency shift ratios are physically possible.

Shown in figure 21 (taken from ref. 7) is the relative change in cavity resonant frequency due to mean flow past the cavity apertures. The results reported in reference 7 are based on an array of resonators tested in a wind tunnel with air. In order to use the results within a rocket engine, the dependency on velocity was converted to a dependency on chamber Mach number. For Mach numbers greater than 0.35, the frequency shift ratio is constant at a value of 1.65 $(1 + (\Delta f/f_o))$. According to reference 7, the frequency shift is a result of the destruction of the laminar flow oscillations in the resonator apertures by turbulence due to the mean flow.

Presented in figure 22 is a plot of the theoretical chamber Mach number as a function of row number or axial distance from the injector. The plot is based on vaporization and combustion of the liquid oxygen and was obtained by the method described in reference 8. The range of velocity profiles considered is due to possible variations in oxygen drop size and other parameters. The results presented indicate that the gas Mach number past the first row of holes is 0.1 or less, while the gas Mach number past the third to eighth row of holes is 0.33. Because of the range of flows considered, the Mach number past the second row can vary from 0.2 to 0.33. For convenience and because of lack of any other information, the solid curve of figure 22 will be used.

Combining the results of figures 21 and 22, the frequency shift ratio for the first row is unity (no flow shift) and for the second to eighth rows, the ratio is 1.63. When it is recalled that the required frequency shift ratio was 1.65, the frequency shift possible due to mean flow satisfies the magnitude requirements for the tuned point frequency shift as well as the restriction that the first row have no frequency shift.

Shown in figure 23 are the results of applying the previously derived frequency shift to the tuning curve of figure 18. For clarity, only the center point of the resonant frequency spread for each cavity depth is shown. The shift ratio simply moves the tuning curve for rows 2 to 8 to a center frequency of 6600 hertz. An analysis of the resulting curves is complicated by the fact that the absorption of a multiply tuned liner (one with more than one tuning point for the same range of cavity depths) has not been fully analyzed. The only conclusion that can be drawn from figure 23 is that the frequency shifts required for tuning a liner to the design frequency seem to be satisfied by flow-induced turbulence in the apertures and that a theoretically calculated chamber gas velocity can be used.

Effect of Liner Length and Position

To separate the effects of liner length (number of rows) and position, two sets of configurations were evaluated with injector IIa. The first set was the first, first and second, and first second and third rows. The objective of these tests was to determine which of the three rows gave the largest contribution to the HTT reduction. The configurations were to be analyzed and plotted as HTT reduction as a function of calculated cavity resonant frequency of the first row. Any significant deviation of the data for the two- and three-row configuration from the curve for the first-row configuration would indicate the contribution of the additional rows.

The second configuration used rows 4 to 8 evaluated at a cavity depth of 13/16 inch (2.06 cm) with injector IIa. The object of testing this configuration was to determine whether rows 4 to 8 could contribute any HTT reduction.

The results of testing partial and full-length liners with injector IIa are presented in figure 24. As with figure 1, each of the data points represents a screech transition point, with the region below each point representing unstable operation. The test variables were mixture ratio, cavity depth, and the number of rows tested.

For each of the configurations tested, the cavity temperatures at transition were measured. The number of thermocouples per row is given in table I. In order to analyze the results, it is necessary to first convert the temperature and cavity depth data to cavity resonant frequencies. Figure 25 shows the axial variation of the transition cavity gas temperatures at a mixture ratio of 5 for all the configurations tested with injector IIa. (Comparison of figs. 12 and 25 shows that the cavity gas temperatures at transition are not greatly different for injectors I and IIa.) The recorded temperatures for the first three rows with injector IIa are indicated by the open circle symbols. The temperatures are tabulated in table III (sections a and b). The cavity resonant frequencies f_o were calculated using the same experimental correlation of gas sonic velocity as a function of cavity gas temperature at transition that was used with the liners tested with injector I (fig. 16).

A plot of HTT reduction against the (nonflow shifted) calculated cavity resonant frequency for the partial-length liners with injector IIa is shown in figure 26. The abscissa is the f_o for the first row only for all the configurations tested. This value was chosen to determine whether the addition of the second or third rows had any effect on the stability of the liner. All the configurations tested seem to fall near a single curve which indicates that, to within the accuracy of the HTT data, the second and third rows had no significant effect on liner absorption.

The calculated frequencies of the rows that did not contribute to the absorption are also tabulated in table III(b). For the configuration b3 in table III, the resonant frequency of the second row was 5100 to 5600 hertz. If a frequency shift factor of 1.65 is used, the flow shifted resonant frequency becomes 8400 to 9280 hertz. Referring to figure 26, a configuration with a resonant frequency in the first row of 8500 to 10 500 hertz should provide between 5 and 15 Rankine degrees (2.78 to 8.33 Kelvin degrees) of HTT reduction. Assuming that the effects of each row were additive, the fact that there was no additional improvement when the second row was tested indicates the higher effectiveness of the first row of holes compared with the second row. This is consistent with the theoretical results presented in figures 18 and 19. However, another aspect is worth noting, namely, that the hydrogen temperature of 5 to 15 Rankine degrees (2.78 to 8.33 Kelvin degrees) noted applied at an initial hydrogen temperature level of 115° R (64° K) when it would produce a change of only 70 percent in hydrogen density and have a corresponding shift in injection velocity ratio. The same change in velocity ratio, but occurring at the lower hydrogen transition temperature obtained with row 1 operative, would correspond to a change of only 2 to 3 Rankine degrees (1.11 to 1.66 Kelvin degrees). Such a small change approaches the available data resolution. Another example is given by the data for configuration b5 of table III where the third row provided no additional stability. The f_o corresponding to a maximum in HTT reduction was approximately 6600 hertz (fig. 26) which is the same design frequency as obtained with injector I. The magnitude of the maximum temperature reduction is 31° R (17.2° K), whereas that obtained with a single row tested with injector I was 36° R (20° K).

In order to determine if any other position than the first row could provide acoustic absorption, a liner with only rows 4 to 8 was tested with injector IIa. The cavity depth was 13/16 inch (2.06 cm) and the results are given in figure 27. At a mixture ratio of 5, the liner provides little or no temperature reduction.

The general conclusion to be drawn from the experiments with partial-length liners is that the greater part of the liner damping is due to the first row. The first row is 3/4 inch (1.91 cm) from the injector face, and the sensitive region for liner operation is apparently closely related to the combustion (or propellant preparation) processes. Consequently, it appears that the stabilization of a combustor may be achieved by an extremely short liner.

Effect of the Injector on Liner Damping

A comparison of first row liner results with injectors I and IIa is shown in figure 28.

Although not large, there are differences in the maximum temperature margin and in the absorption bandwidth. In order to analyze the results, a model for the operation of the liners must be assumed. The results of reference 1 indicate that the acoustic absorption coefficient α can characterize the damping of an acoustic liner. The only measured difference between the two injectors, which could, theoretically, result in different values of the acoustic absorption coefficient, is the difference in the amplitude of 6600-hertz design frequency in the pretransition period. Referring to figure 8, the amplitude of the 6600-hertz signal for injector I is 5 psi (34.5 kN/m^2) and for injector IIa, 0.5 psi (3.45 kN/m^2).

The absorption coefficients are calculated by the method presented in references 1, 2, and 9. The results are shown in figure 29. The parameters varied in the calculation were the wave amplitude and the wave frequency. Figure 29 shows that the liner operating with injector I has a much wider bandwidth and higher peak absorption.

There are several assumptions associated with the calculation, and the absolute value of the absorption coefficient does not have great significance. The difference between the two theoretical values, however, is significant, and appears to be consistent with the experimental results.

To determine the effect of injector type on the operation of an eight-row liner, an eight-row liner with a cavity depth of 13/16 inch (2.06 cm) was stability rated with injector IIa. The results of testing an eight-row liner with injector I at a cavity depth of 13/16 inch (2.06 cm) are presented in figure 9. For comparison, both liner results are shown in figure 30. The hydrogen-temperature margin (at a mixture ratio of 5) for the liner with injector I was 33° R (18.35° K), and the hydrogen-temperature margin for the liner with injector IIa was 18° R (10° K).

The cavity transition temperatures and the calculated resonant frequencies for both configurations are tabulated in tables II and III (section c in both). The axial variation of calculated resonant frequencies is shown in figure 31. The results presented in figure 31 indicate that the two configurations had the same average resonant frequency, and the difference in damping or temperature margin can be attributed to differences in the liner absorption coefficient as indicated by figure 29.

The conclusion to be drawn from the comparison of the full- and partial-length liners with the two injectors is that experimental differences, in both cases, can be explained by differences in the liner acoustic absorption coefficient.

SUMMARY OF RESULTS

1. Discrete oscillations generally appear in the chamber before transition at considerably lower amplitudes than the screech wave and at different frequencies.

2. In order to have the liner resonant frequency at tuning agree with the predominant pretransition frequency, a frequency shifting mechanism was required.

3. A theoretically predicted mean axial flow variation, in conjunction with the frequency shifting curve of reference 7, satisfied the frequency shifting requirements for tuning.

4. There is considerably more hydrogen in the liner cavities than would have been predicted from the results of reference 1.

5. Varying the cavity volume of a resonator produced a peak value in damping based on hydrogen transition temperature reduction.

6. The difference in the effectiveness of the same liner with two different injectors can be explained by the difference in the pretransition oscillation amplitudes of the two injectors and the resulting difference in the theoretical acoustic absorption coefficient.

7. The damping at rows 2 and 3 was negligible compared with row 1. Rows 4 to 8 contribute little or no damping.

8. The ratio of aperture area to internal resonator cross-sectional area appeared to correlate cavity gas temperature at transition.

Lewis Research Center,
National Aeronautics and Space Administration,
Cleveland, Ohio, November 16, 1967,
128-31-06-05-22.

APPENDIX - BASIC EQUATIONS

Resonant Frequency of Helmholtz Resonator

$$f_o = \frac{12c}{2\pi}\sqrt{\frac{\sigma_i}{l_{eff}\, l}} \qquad \text{(A1)}$$

where f_o is the calculated resonant frequency, c is the sonic velocity, σ_i is the ratio of neck area to cavity cross-sectional area, l is the cavity depth, and l_{eff} is the effective liner thickness or neck length which is a function of gas velocity.

For zero gas velocity (ref. 1),

$$\left.\begin{aligned} l_{eff} &= t + \delta l_{eff} \\ \delta l_{eff} &= 0.85\, d\left(1 - 0.7\sqrt{\sigma_i}\right) \end{aligned}\right\} \qquad \text{(A2)}$$

where d is the diameter of the circular apertures and t is the liner thickness.

Sonic Velocity

$$c = 298.8\sqrt{\frac{\gamma T}{\mathscr{M}}} \qquad \text{(A3)}$$

where γ is the specific heat ratio (cp/cv), T is the absolute temperature, and $\mathscr{M}$ is the molecular weight.

Average Molecular Weight

$$\mathscr{M} = \sum_{i=1}^{N} X_i \mathscr{M}_i \qquad \text{(A4)}$$

where $\mathscr{M}_i$ is the molecular weight of species i and X_i is the molecular fraction of species i.

REFERENCES

1. Wanhainen, John P.; Bloomer, Harry E.; Vincent, David W.; and Curley, Jerome K.: Experimental Investigation of Acoustic Liners to Suppress Screech in Hydrogen-Oxygen Rockets. NASA TN D-3822, 1967.
2. Vincent, David W.; Phillips, Bert; and Wanhainen, John P.: Acoustic Liners to Suppress Screech in Storable Engines. NASA TN D-4442, 1968.
3. Svehla, Roger A.: Thermodynamic and Transport Properties for the Hydrogen-Oxygen System. NASA SP-3011, 1964.
4. F-1 Acoustic Absorber: Contract no. NASw-16. Monthly Progress Report no. 7, December 12, 1966.
5. Wanhainen, John P.; Parish, Harold C.; and Conrad, E. William: Effect of Propellant Injection Velocity on Screech in 20 000-Pound Hydrogen-Oxygen Rocket Engine. NASA TN D-3373, 1966.
6. Phillips, Bert; and Morgan, C. Joe: Mechanical Absorption of Acoustic Oscillations in Simulated Rocket Combustion Chambers. NASA TN D-3792, 1967.
7. Mechel, F.; Mertens, P.; and Schilz, W.: Research on Sound Propagation in Sound-Absorbent Ducts with Superimposed Air Streams. Final Rep. (AMRL-TDR-62-140, vol. III), Physikalisches Inst., Univ. Göttingen, West Germany, Dec. 1962.
8. Priem, Richard J.; and Heidmann, Marcus F.: Propellant Vaporization as a Design Criterion for Rocket-Engine Combustion Chambers. NASA TR R-67, 1960.
9. Ingard, Uno: On the Theory and Design of Acoustic Resonators. Acoust. Soc. Am. J., vol. 25, no. 6, Nov. 1953, pp. 1037-1061.

TABLE I. - CONFIGURATIONS EVALUATED

[Liner thickness, 3/16 in. (0.476 cm); diameter of circular apertures, 1/4 in. (0.685 cm); ratio of neck area to cross-sectional area, 0.121.]

(a) U. S. customary units

Injector	Row	Cavity depth, in.	Cavity gas thermocouples per row
I	1 - 8	$\frac{5}{16}$, $\frac{9}{16}$, $\frac{13}{16}$, $1\frac{1}{16}$, $1\frac{13}{16}$, 3.2	[a]1
	1	$\frac{9}{16}$, $\frac{13}{16}$, $1\frac{1}{16}$	2
IIa	1	$\frac{9}{16}$	2
	[b]2	$\frac{9}{16}$, $\frac{13}{16}$, $1\frac{1}{16}$	2
	[c]3	$\frac{13}{16}$, $1\frac{13}{16}$	2
	1 - 8	$\frac{13}{16}$	
	1	$\frac{5}{16}$, $\frac{9}{16}$, $\frac{13}{16}$, $1\frac{5}{16}$, $2\frac{5}{16}$	4
	4 - 8	$\frac{13}{16}$	
IIb	3	$\frac{5}{16}$, $\frac{15}{16}$, $2\frac{5}{16}$, 3.2	[d]4

[a]For cavity depths of $\frac{13}{16}$ and $1\frac{13}{16}$ in. (2.064 and 4.604 cm). Only the first three rows were instrumented.

[b]Tested while row 1 liner was at 9/16 in. (1.429 cm).

[c]Tested while liner rows 1 and 2 were held constant at 9/16 in. (1.429 cm).

[d]Gas sampling.

TABLE I. - Concluded. CONFIGURATIONS EVALUATED

[Liner thickness, 3/16 in. (0.476 cm); diameter of circular apertures, 1/4 in. (0.685 cm); ratio of neck area to cross-sectional area, 0.121.]

(b) SI units

Injector	Row	Cavity depth, cm	Cavity gas thermocouples per row
I	1 - 8	0.794, 1.429, 2.064, 2.699, 4.603, 8.128	[a]1
	1	1.429, 2.054, 2.699	2
IIa	1	1.429	2
	[b]2	1.429, 2.064, 2.699	2
	[c]3	2.064, 4.603	2
	1 - 8	2.064	1
	1	0.794, 1.429, 2.064, 3.334, 5.874	4
	4 - 8	2.064	1
IIb	3	0.194, 3.334, 5.874, 8.128	[d]4

[a]For cavity depths of $\frac{13}{16}$ and $1\frac{13}{16}$ in. (2.064 and 4.604 cm). Only the first three rows were instrumented.
[b]Tested while row 1 liner was at 9/16 in. (1.429 cm).
[c]Tested while liner rows 1 and 2 were held constant at 9/16 in. (1.429 cm).
[d]Gas sampling.

TABLE II. - INJECTOR I: CAVITY PROPERTIES AT TRANSITION

[Mixture ratio, 5.]

(a) U. S. customary units

Section	Configuration		Cavity gas temperature at transition, ^{o}R	Calculated cavity resonant frequency, f_o, Hz	Hydrogen temperature margin, ^{o}R
	Row	Cavity depth, in.			
a	1	$1\frac{13}{16}$	400 - 740	3000 - 4250	48
	2		500 - 700	3400 - 4100	
	3		600 - 800	4100 - 4400	
	4		650 - 1000	3950 - 4400	
	5		630 - 850	3850 - 4400	
	6		700 - 800	4100 - 4400	
	7		680 - 950	3500 - 4400	
	8		600 - 900	3850 - 4400	
b	1	$\frac{9}{16}$	[a]635	7150	36
	1	$\frac{13}{16}$	489 - 626	5150 - 5760	30
	1	$1\frac{1}{16}$	431 - 506	4300 - 4500	24
c	1	$\frac{13}{16}$	400 - 740	4500 - 6400	34
	2		500 - 700	5150 - 6150	
	3		600 - 800	6150 - 6600	
	4		650 - 1000	4950 - 6600	
	5		630 - 850	4800 - 6600	
	6		700 - 800	5150 - 6600	
	7		680 - 950	4400 - 6600	
	8		600 - 900	4450 - 6600	

[a]Identical readings.

TABLE II. - Concluded. INJECTOR I: CAVITY PROPERTIES AT TRANSITION

[Mixture ratio, 5.]

(b) SI units

Section	Configuration		Cavity gas temperature at transition, °K	Calculated cavity resonant frequency, f_o, Hz	Hydrogen temperature margin, °K
	Row	Cavity depth, cm			
a	1	4.604	222 - 411	3000 - 4250	27
	2		278 - 389	3400 - 4100	
	3		333 - 444	4100 - 4400	
	4		361 - 555	3950 - 4400	
	5		350 - 472	3850 - 4400	
	6		389 - 444	4100 - 4400	
	7		378 - 528	3500 - 4400	
	8		378 - 500	3850 - 4400	
b	1	1.429	[a]353	7150	20
	1	2.064	272 - 348	5150 - 5760	17
	1	2.699	239 - 281	4300 - 4500	13
c	1	2.064	222 - 411	4500 - 6400	19
	2		278 - 389	5150 - 6150	
	3		333 - 444	6150 - 6600	
	4		361 - 555	4950 - 6600	
	5		350 - 472	4800 - 6600	
	6		389 - 444	5150 - 6600	
	7		378 - 528	4400 - 6600	
	8		333 - 500	4450 - 6600	

[a]Identical readings.

TABLE III. - INJECTOR IIa: CAVITY PROPERTIES AT TRANSITION

[Mixture ratio, 5.]

(a) U.S. customary units

Section	Configuration		Cavity gas temperature at transition, °R	Calculated cavity no flow shift resonant frequency, f_o, Hz	Hydrogen temperature margin, °R
	Row	Cavity depth, in.			
a	1	$\frac{9}{16}$	600, 608	6800	10
	1	$\frac{9}{16}$	613, 570, 683, 392	5600 - 7300	31
	1	$\frac{5}{16}$	595, 904, 869, 490	8300 - 10 000	15
	1	$\frac{13}{16}$	622, 574, 608, 559	5450 - 6150	23
	1	$1\frac{5}{16}$	509, 857, 616, 414	3820 - 5200	21
	1	$2\frac{5}{16}$	689, 696, 891, 680	3600 - 3900	21
b 1	1	$\frac{9}{16}$	571, 581	6650	13
	2	$\frac{9}{16}$	622, 667	7000 - 7250	13
b 2	1	$\frac{9}{16}$	544, 563	6400 - 6600	15
	2	$\frac{13}{16}$	620, 698	5750 - 6150	15
b 3	1	$\frac{9}{16}$	567, 584	7100 - 7500	15
	2	$1\frac{1}{16}$	629, 748	5100 - 5600, [a]8400 - 9280	15
b 4	1	$\frac{5}{16}$	692, 727	7400 - 7700	15
	2	$\frac{9}{16}$	875, 880	6650	15
	3	$\frac{13}{16}$	698, 730	6150 - 6350	15
b 5	1	$\frac{9}{16}$	465, 582	6050 - 6700	30
	2	$\frac{9}{16}$	615, 618	6950	30
	3	$1\frac{13}{16}$	601, 627	3760 - 3900, [a]6200 - 6440	

[a]Frequency shifted by a factor of 1.63.

TABLE III. - Continued. INJECTOR IIa: CAVITY PROPERTIES

AT TRANSITION

[Mixture ratio, 5.]

(a) Concluded. U.S. customary units

Section	Configuration		Cavity gas temperature at transition, ^{o}R	Calculated cavity no flow shift resonant frequency, f_o, Hz	Hydrogen temperature margin, ^{o}R
	Row	Cavity depth, in.			
c	1	$\frac{13}{16}$	600	5650	20
	2		950	5270	
	3		990	5340	
	4		980	5340	
	5		960	5270	
	6		885	5450	
	7		835	6280	
	8		720	6280	
d	4	$\frac{13}{16}$	760	6460	7
	5		800	6600	
	6		970	5340	
	7		970	5340	
	8		830	6280	

TABLE III. - Concluded. INJECTOR IIa: CAVITY PROPERTIES AT TRANSITION

[Mixture ratio, 5.]

(b) SI units

Section	Configuration		Cavity gas temperature at transition, °K	Calculated cavity no flow shift resonant frequency, f_o, Hz	Hydrogen temperature margin, °K
	Row	Cavity depth, cm			
a	1	1.429	333, 338	6800	6
	1	1.429	341, 317, 379, 218	5600 - 7300	17
	1	.794	331, 502, 483, 272	8300 - 10 000	8
	1	2.064	346, 319, 382, 311	5450 - 6150	13
	1	3.334	283, 476, 342, 230	3820 - 5200	12
	1	5.874	383, 387, 495, 378	3600 - 3900	12
b 1	1	1.429	317, 323	6650	7
	2	1.429	346, 371	1111 - 4028	7
b 2	1	1.429	302, 313	6400 - 6600	8
	2	2.064	344, 388	5750 - 6150	8
b 3	1	1.429	315, 324	7100 - 7500	8
	2	2.699	349, 416	5100 - 5600, [a]8400 - 9280	8
b 4	1	1.429	384, 434	7400 - 7700	8
	2	1.429	488, 489	6650	8
	3	2.064	388, 406	6150 - 6350	8
b 5	1	1.429	261, 323	6050 - 6700	17
	2	1.429	342, 343	6950	17
	3	4.604	334, 348	3760 - 3900, [a]6200 - 6440	17
c	1	2.064	333	5650	11
	2	↓	528	5270	↓
	3	↓	550	5340	↓
	4	↓	544	5340	↓
	5	↓	500	5270	↓
	6	↓	492	5450	↓
	7	↓	464	6280	↓
	8	↓	400	5280	↓
d	4	2.064	422	6460	7
	5	↓	444	6600	↓
	6	↓	539	5340	↓
	7	↓	539	5340	↓
	8	↓	461	6280	↓

[a]Frequency shifted by a factor of 1.63.

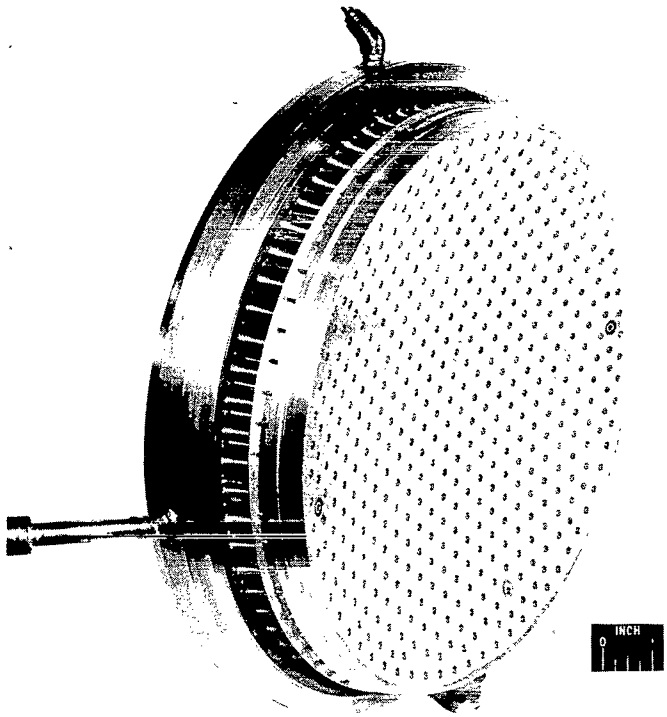

C-72129

(a) Injector I.

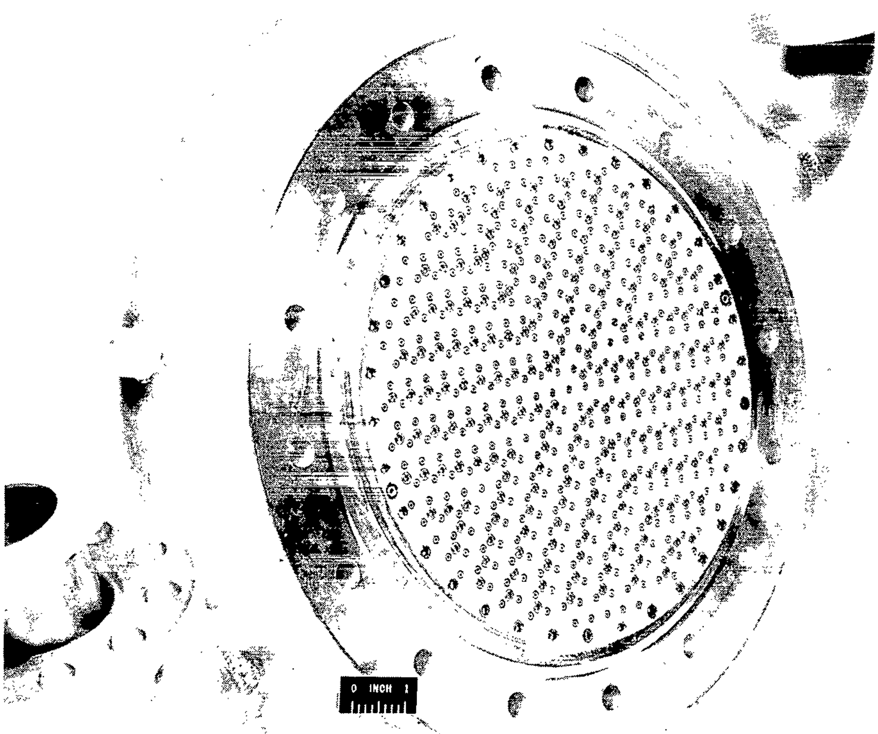

C-73221

(b) Injector IIa.

Figure 1. - Concentric tube injectors.

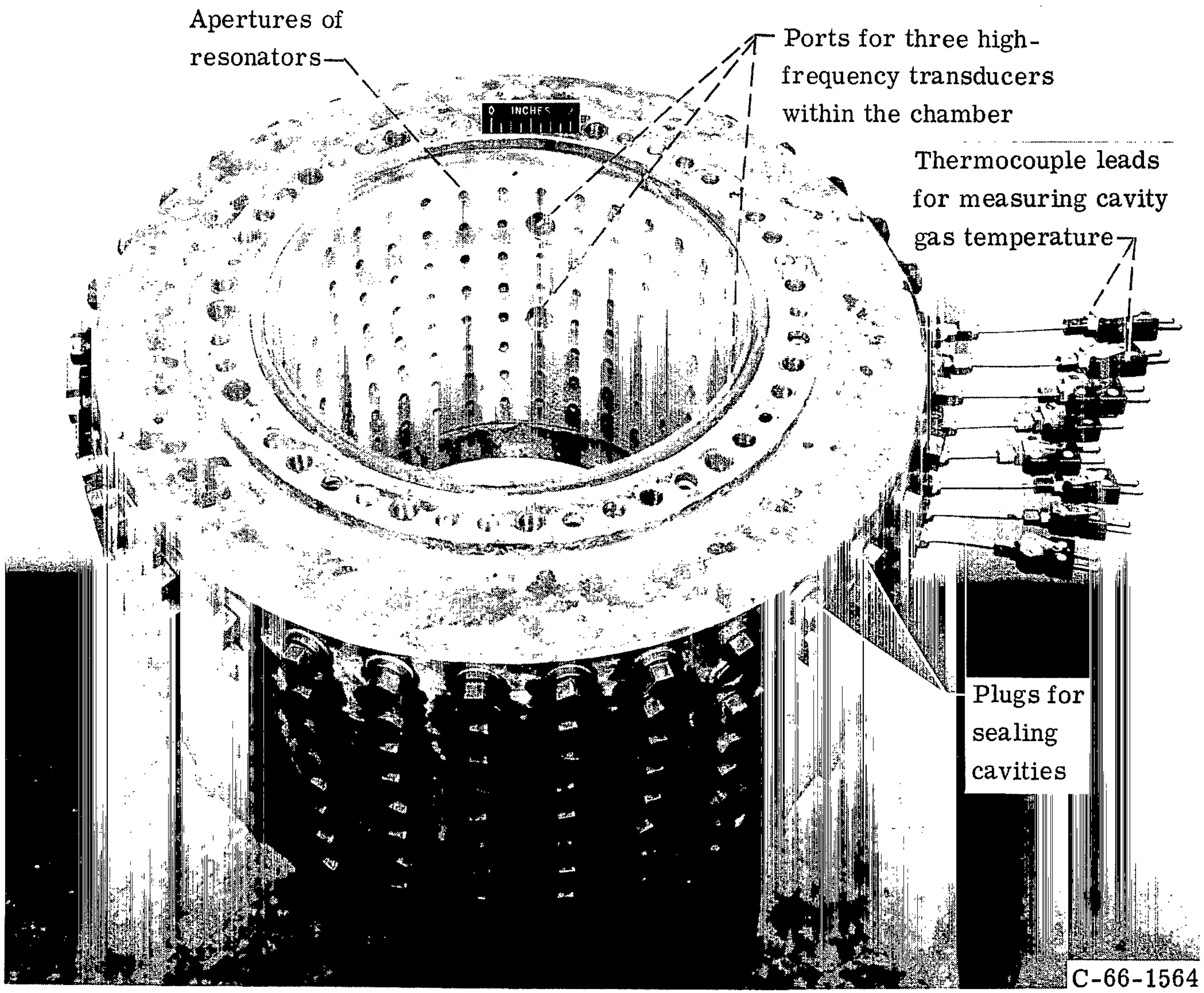

Figure 2. - Jacket and liner.

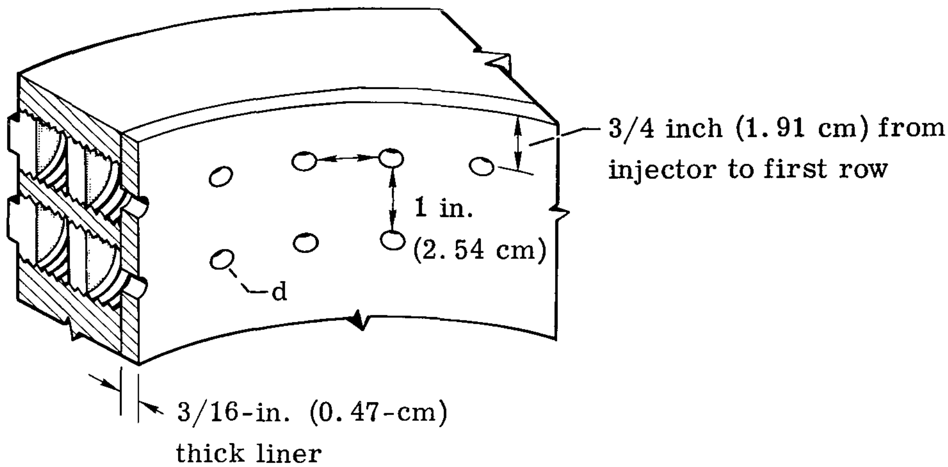

(a) Liner with jacket.

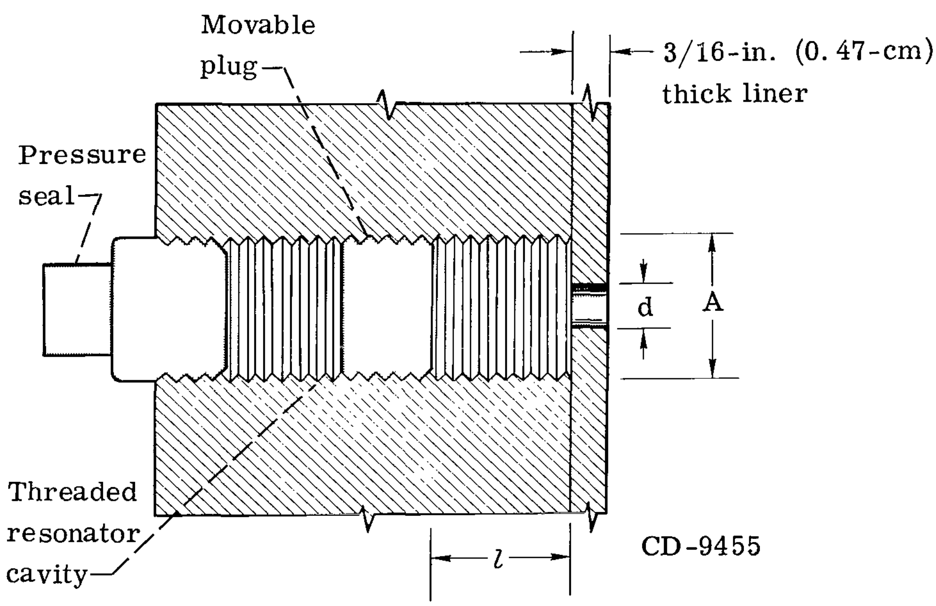

(b) Detail of single cavity.

Figure 3. - Details of liner and cavity. Full-length, eight-row liner, 34 rows per hole. Hole spacing, 1 by 1 inch (2.54 by 2.54 cm); internal open area ratio, 0.121; external open area ratio, 0.05; hole diameter, d, 1/4 inch (0.035 cm); liner thickness, t, 3/16 inch (0.47 cm); resonator internal diameter, A, 23/32 inch (1.825 cm); cavity depth, l, 0 to 3.2 inch (0 to 8.13 cm).

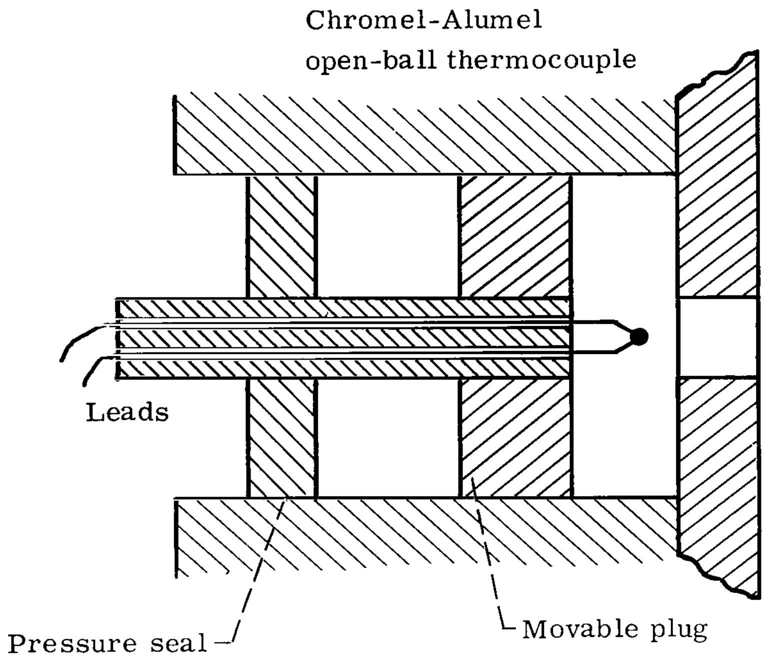

(a) Detail of modification for cavity-gas temperature measurement.

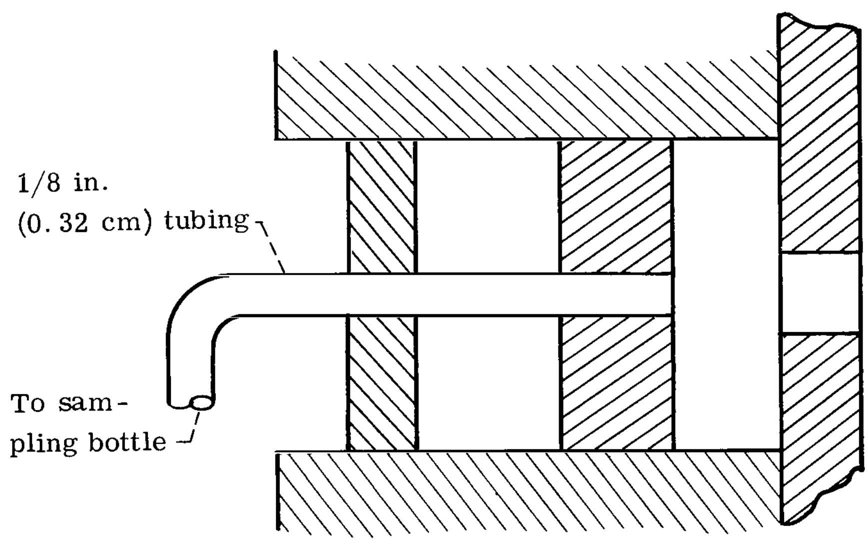

(b) Detail of modification for gas sampling.

Figure 4. - Detail of modified cavities in variable cavity depth liner.

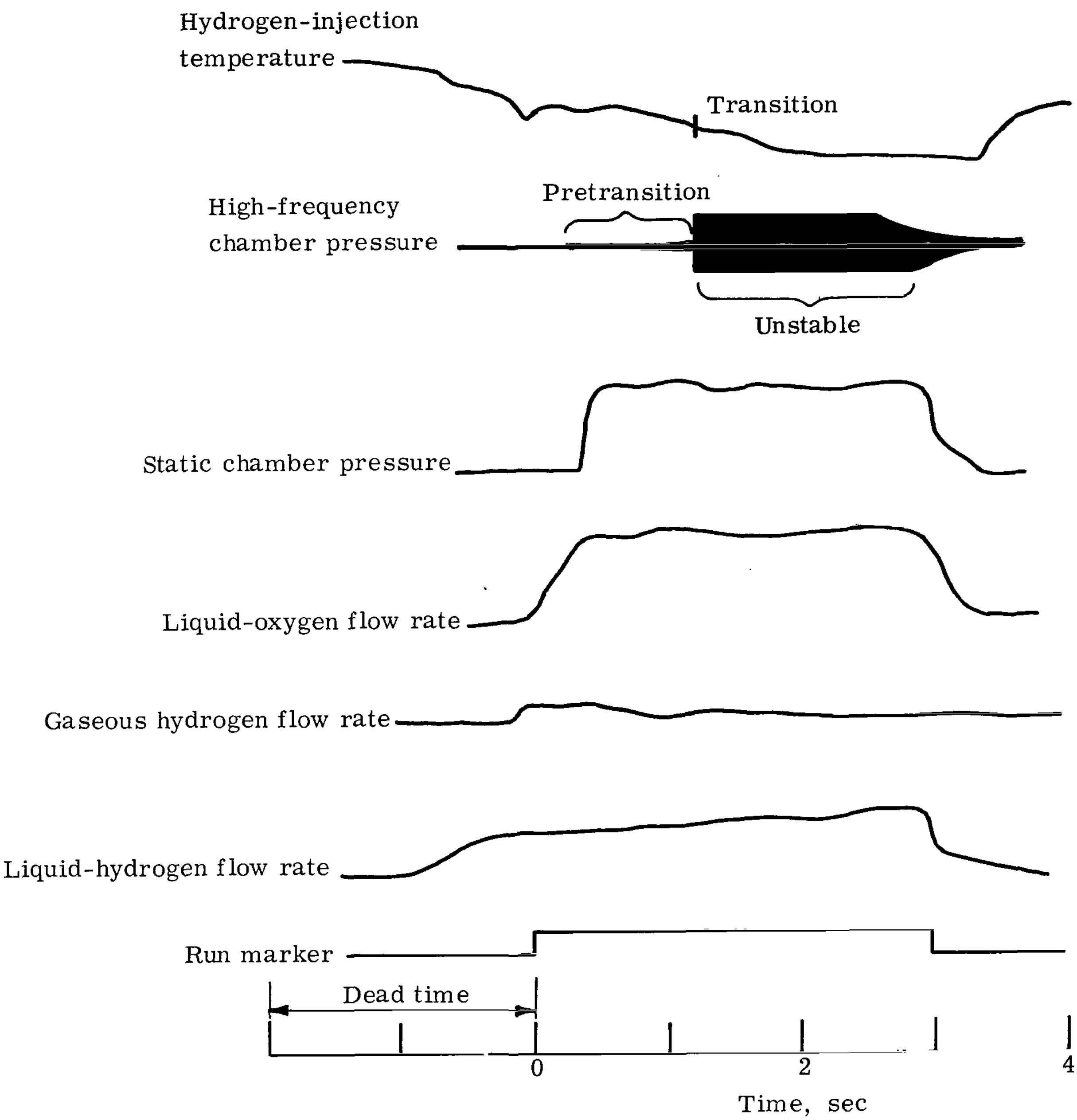

Figure 5. - Typical screech rating test.

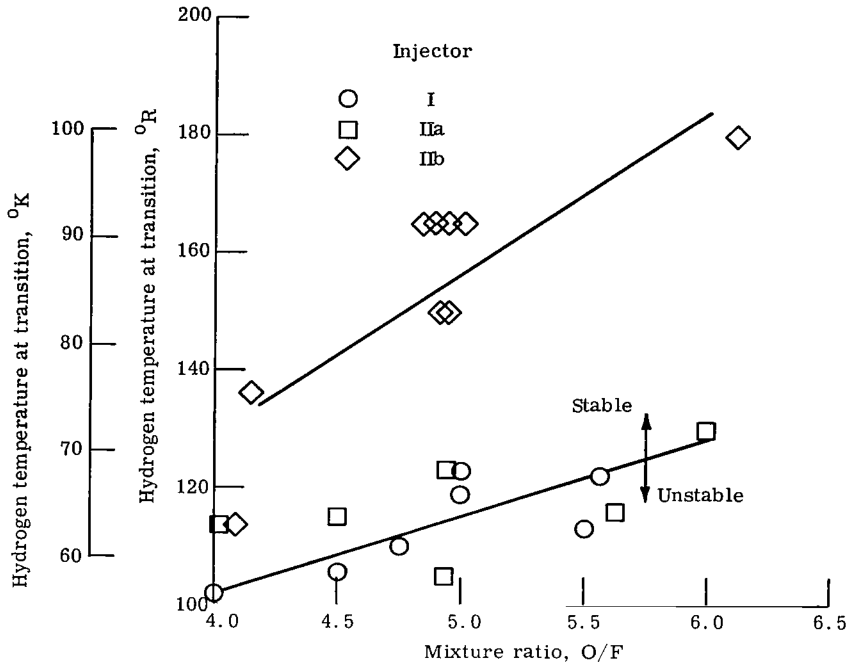

Figure 6. - Hydrogen temperature stable operating limits of engine without liner (base lines).

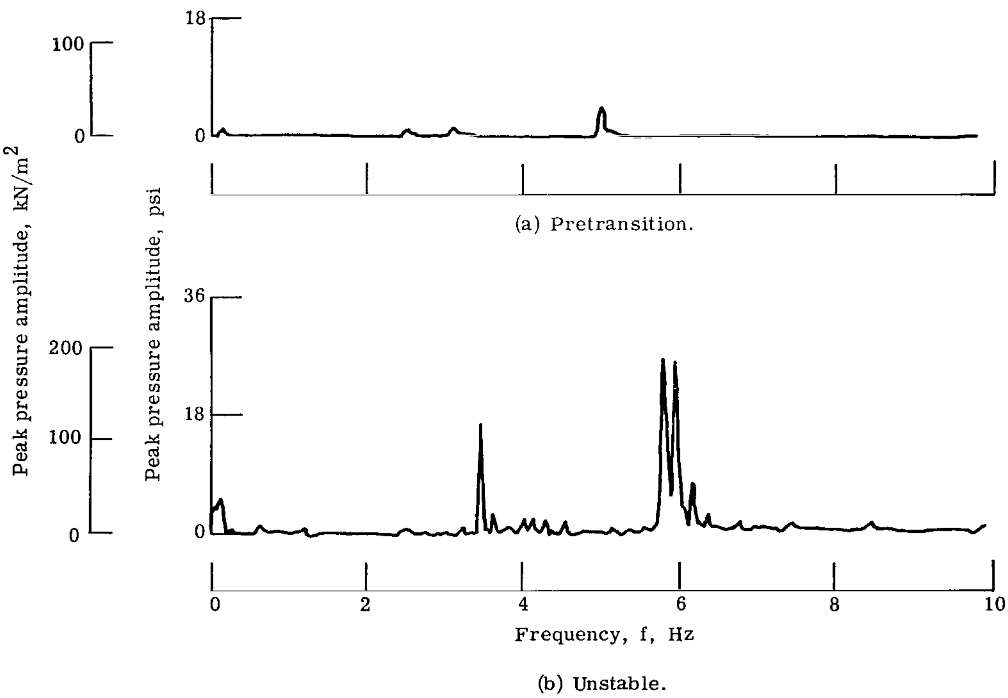

Figure 7. - Amplitude spectral analysis of high-frequency transducer data. Injector I; mixture ratio, 5.

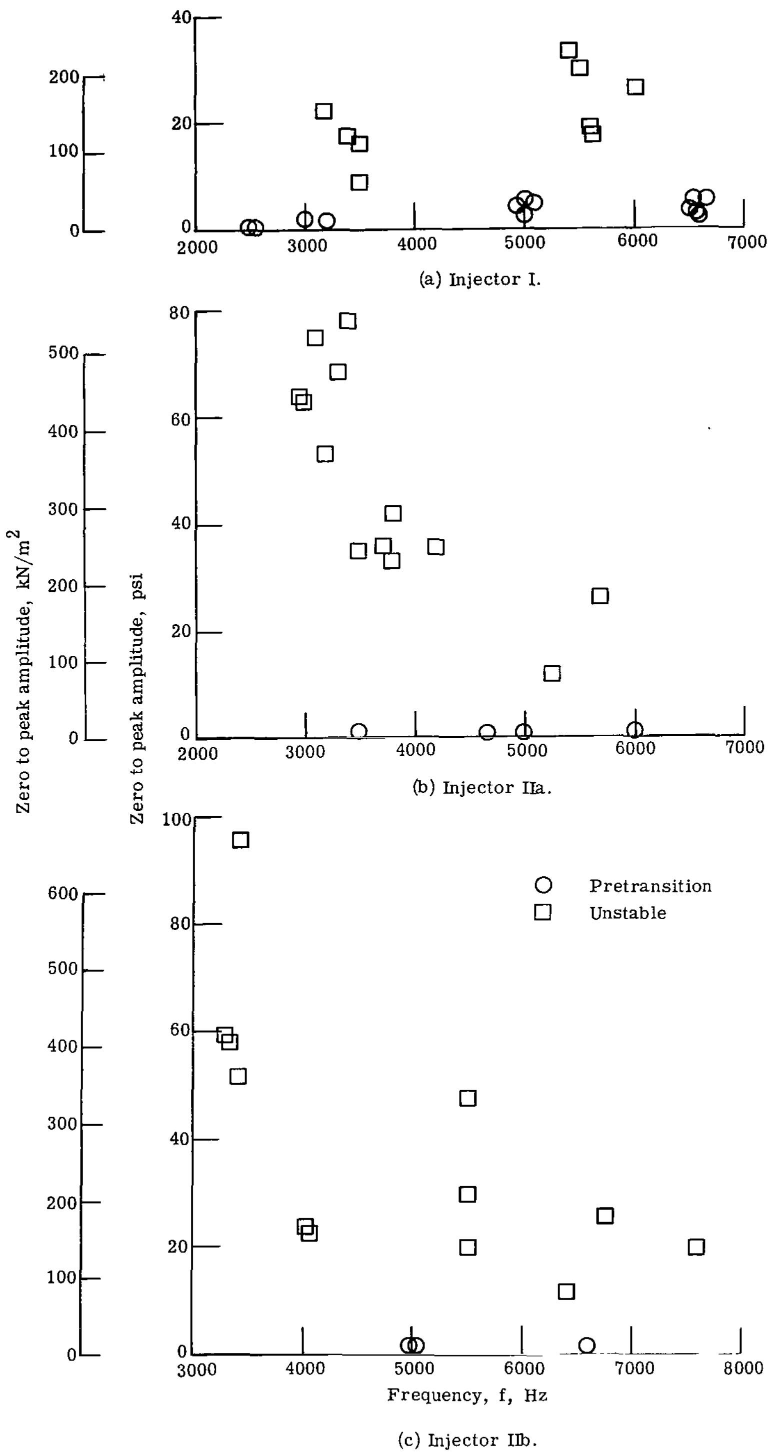

Figure 8. - Maximum amplitude for pretransition and unstable periods. No liner; mixture ratio, 4 to 6.

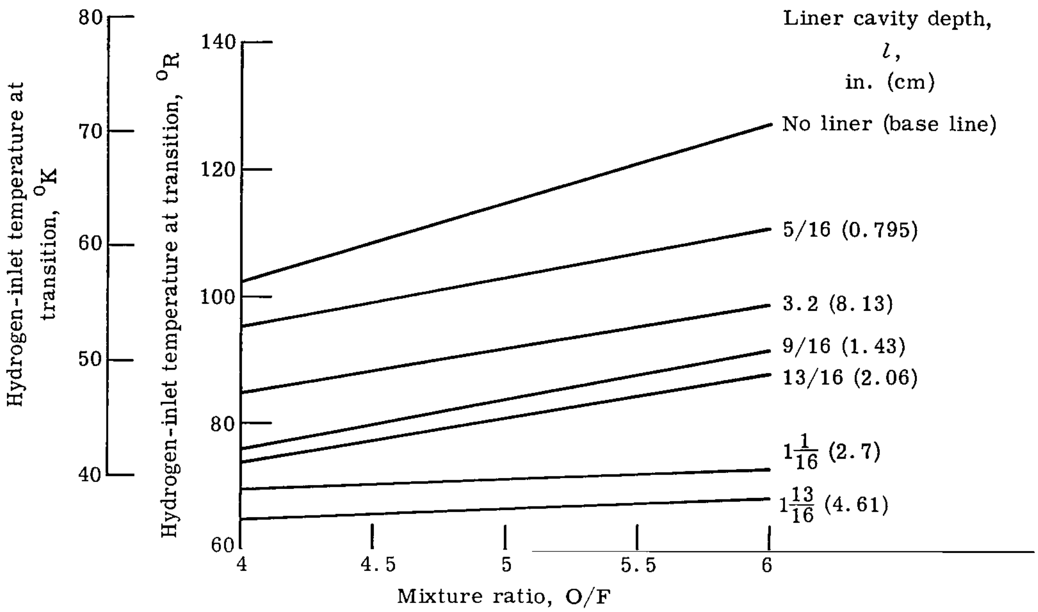

Figure 9. - Hydrogen transition temperature for eight-row liner and injector I.

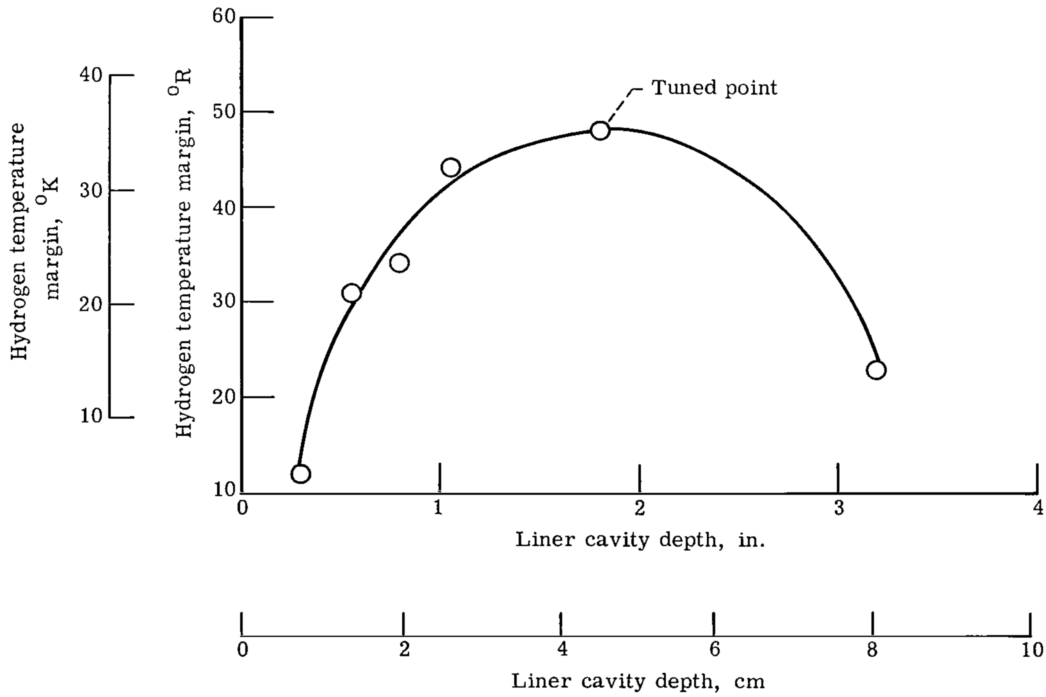

Figure 10. - Hydrogen temperature margin as function of liner cavity depth. Mixture ratio, 5; number of rows, 8; injector I.

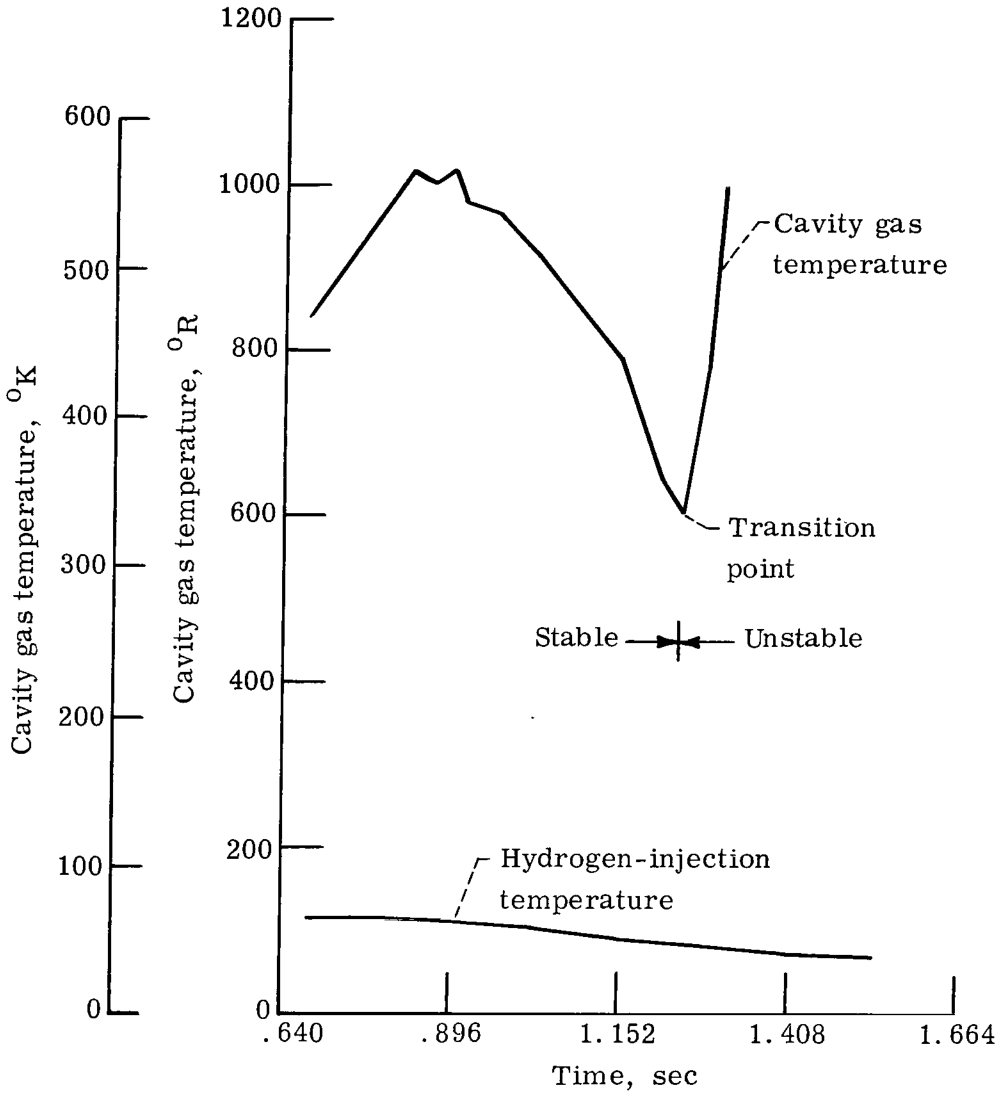

Figure 11. - Time history of typical cavity gas temperature and hydrogen-injection temperature. Mixture ratio, 4.49; injector IIa; full-length eight-row liner; liner cavity depth, 13/16 inch (2.06 cm). Measurement made $1\frac{1}{2}$ inches (3.81 cm) from injector face.

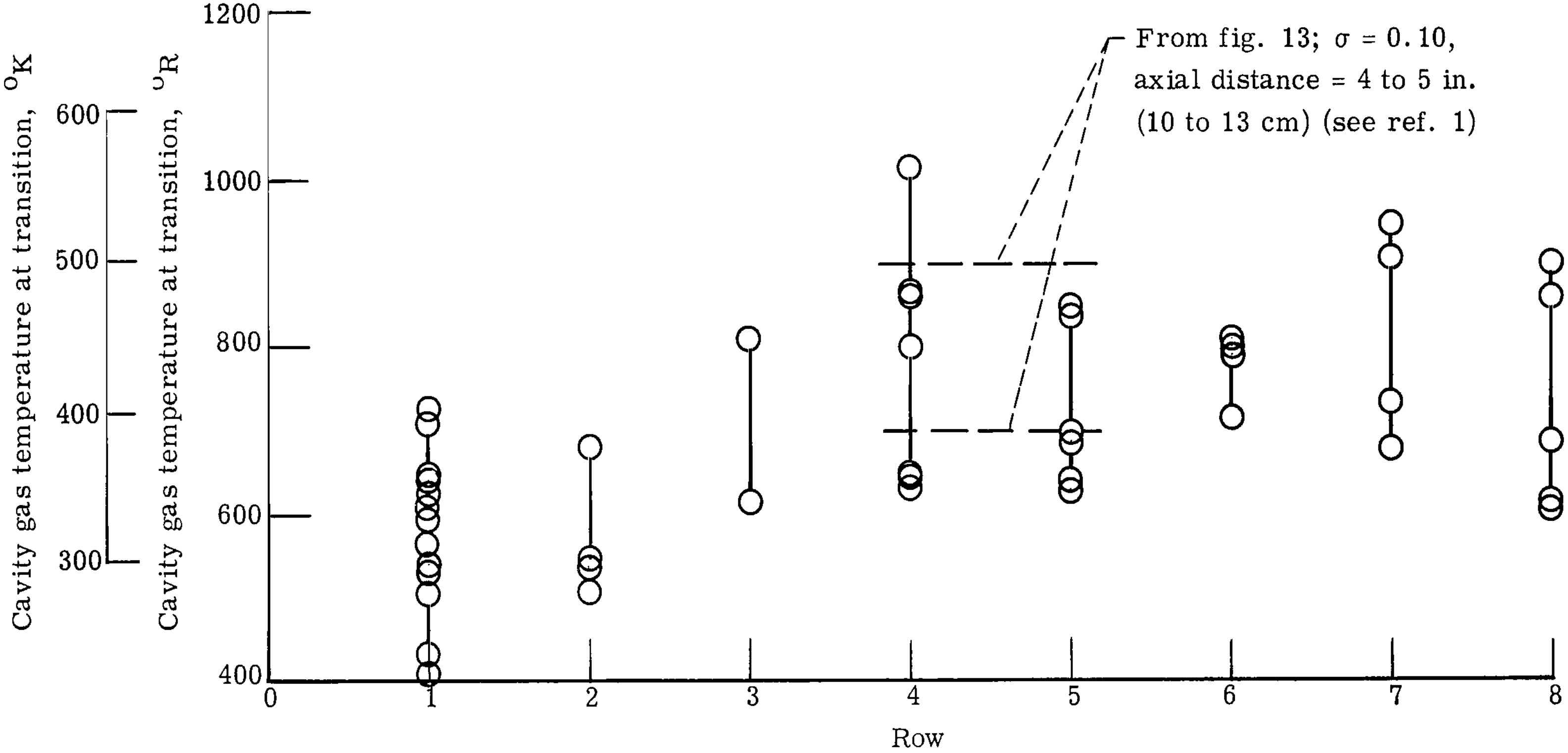

Figure 12. - Axial variation of cavity-gas temperature at transition. Injector I; mixture ratio, 5. Data spread is due to variation in cavity gas temperature for all cavity depths.

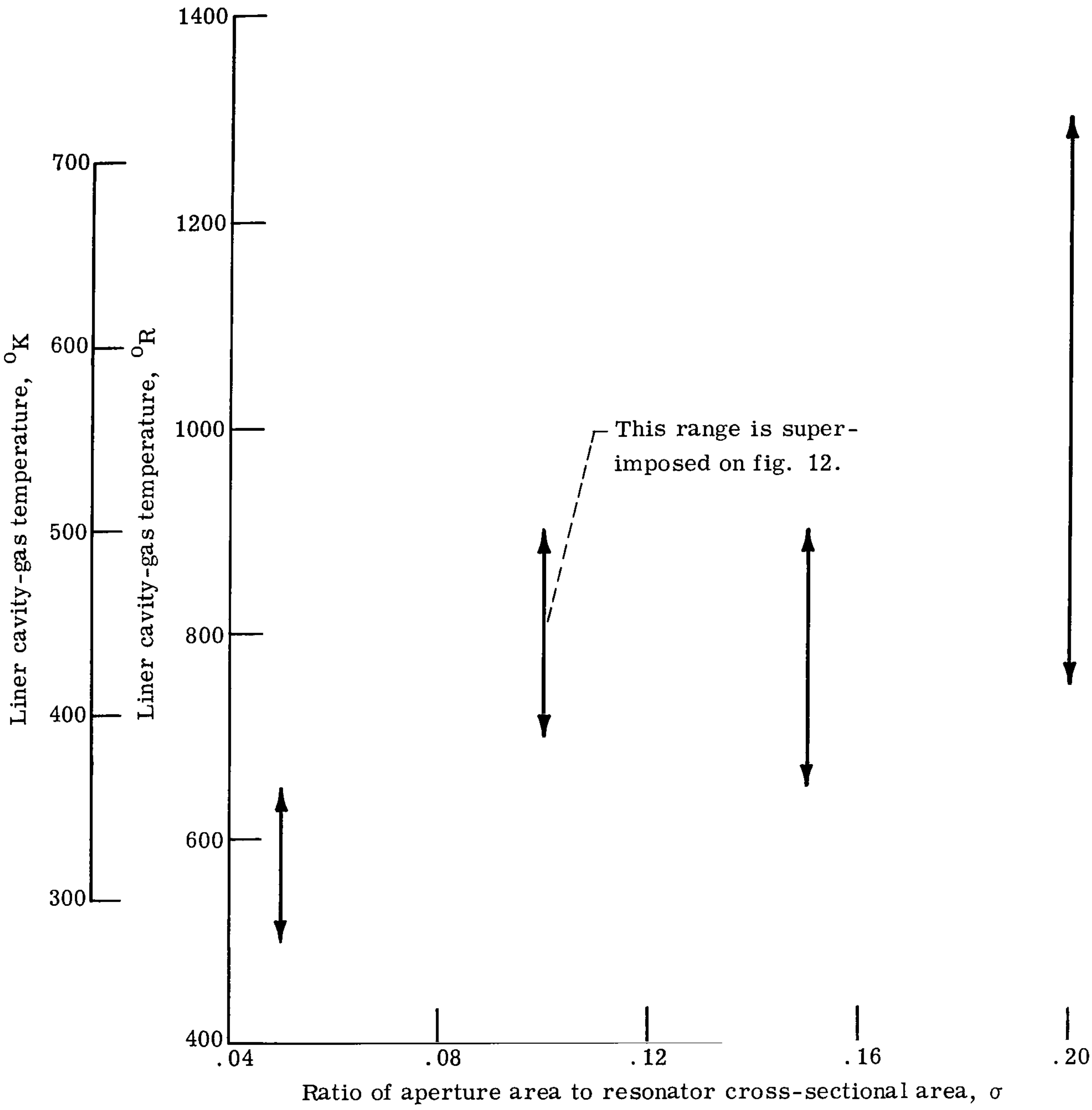

Figure 13. - Liner cavity gas temperature as function of ratio of aperture area to resonator cross-sectional area. Axial distance from injector, 4 to 5 inches (10 to 12.5 cm). (This figure was taken from ref. 1.)

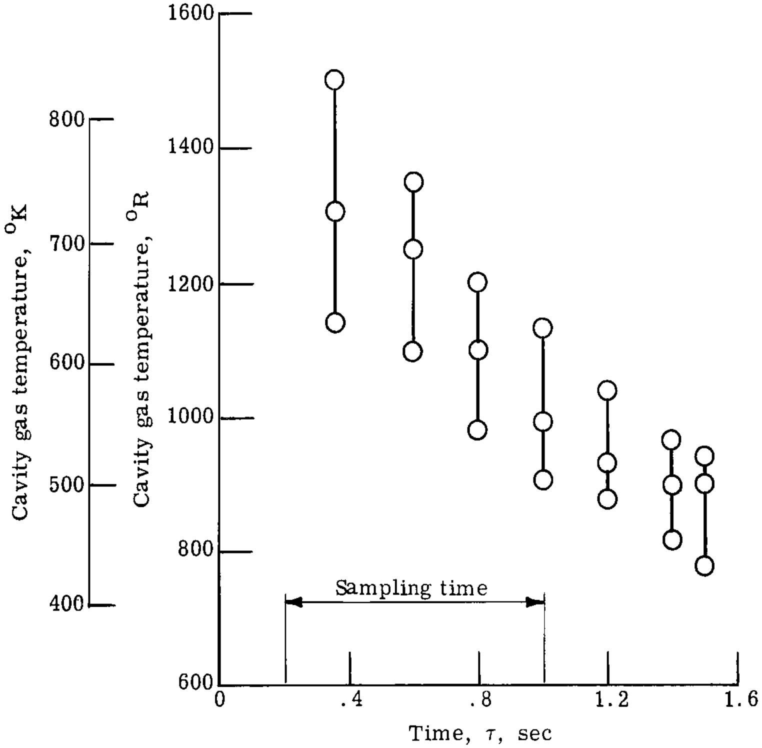

Figure 14. - Variation of cavity gas temperature with time during gas sampling test run. Mixture ratio, 4.91; cavity depth, $1\frac{5}{16}$ inch (3.34 cm); injector IIb; row 3.

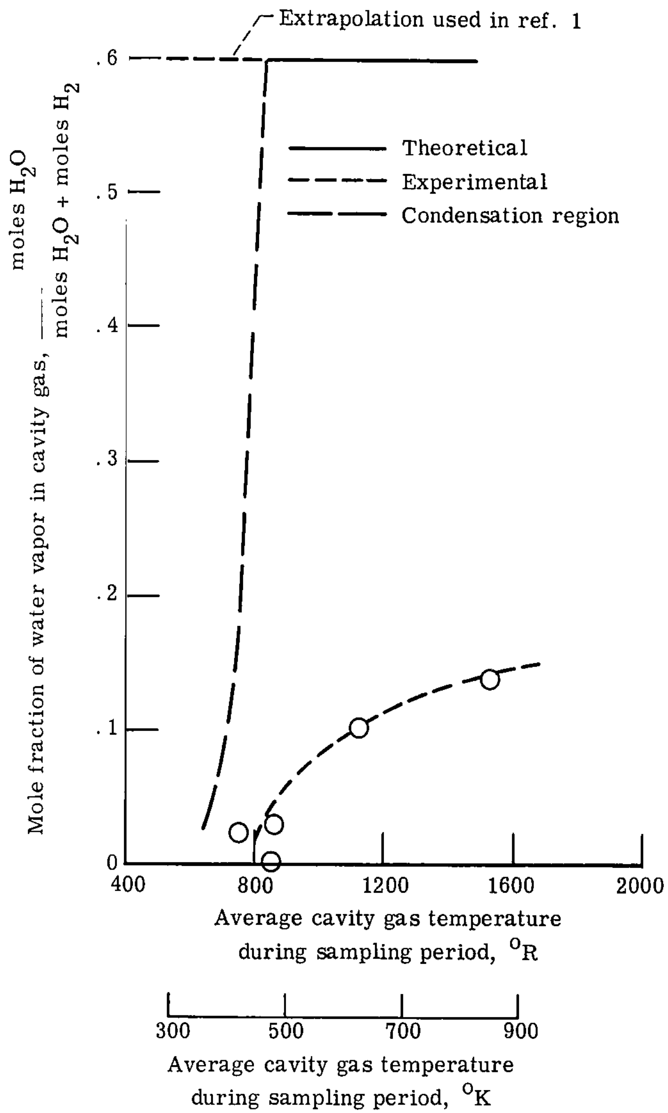

Figure 15. - Cavity gas composition as function of cavity gas temperature. Injector IIb; row 3; mixture ratio, 5; cavity depth, 7/16 to 3.2 inches (1.11 to 8.12 cm).

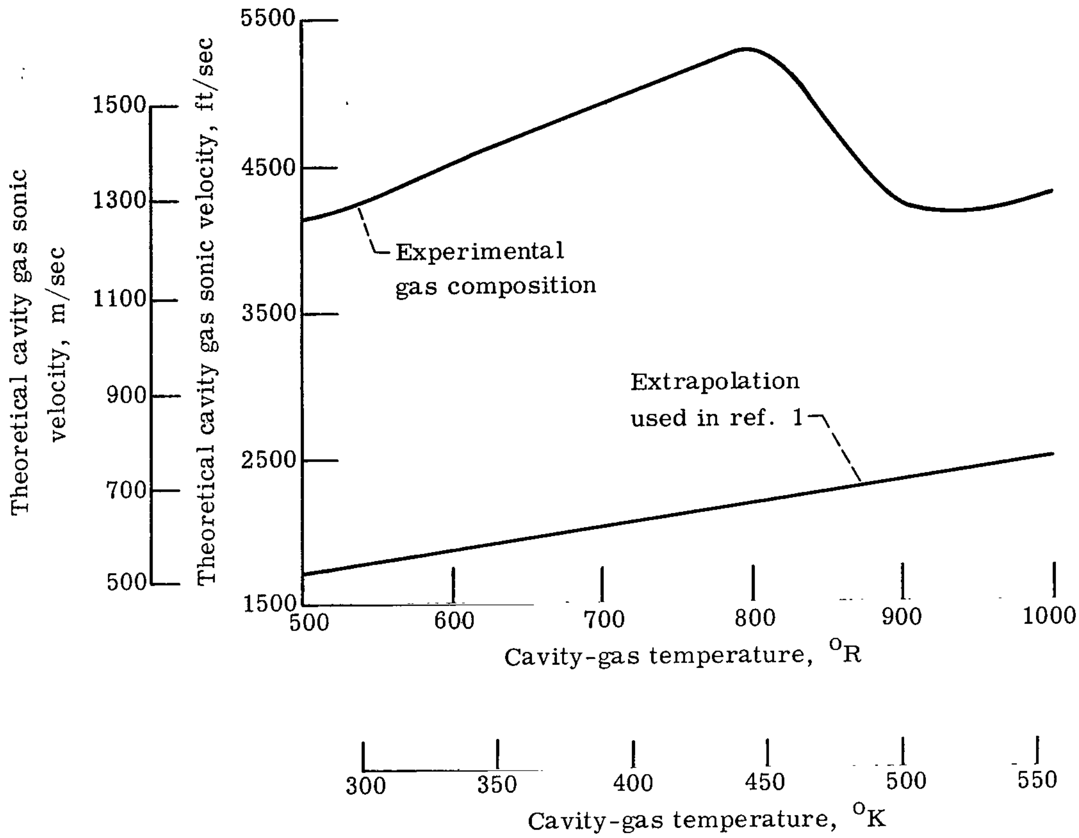

Figure 16. - Theoretical cavity-gas sonic velocity as function of cavity-gas temperature.

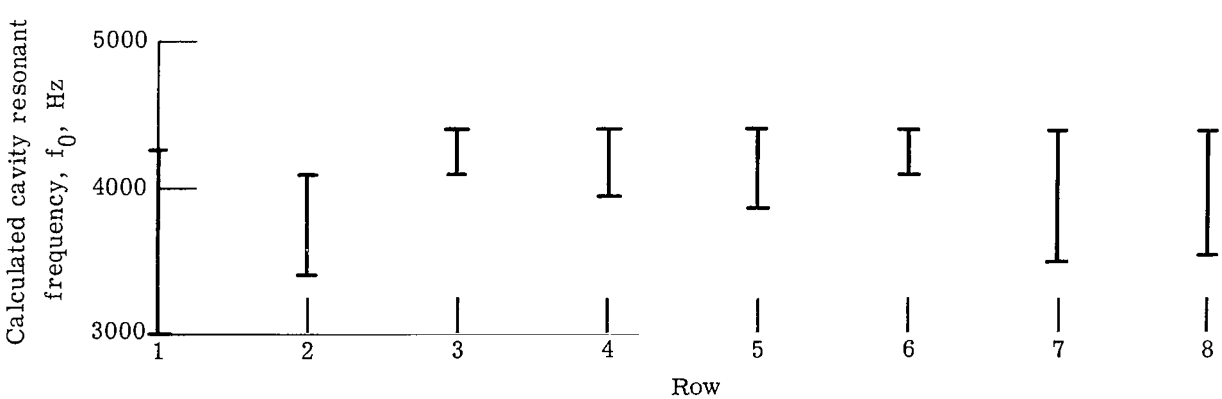

Figure 17. - Calculated resonant frequency for each row based on cavity temperature spread at transition. Injector I; full-length, eight-row liner. Mixture ratio, 5; cavity depth, $1\frac{13}{16}$ inches (4.61 cm). Data spread due to temperature variation.

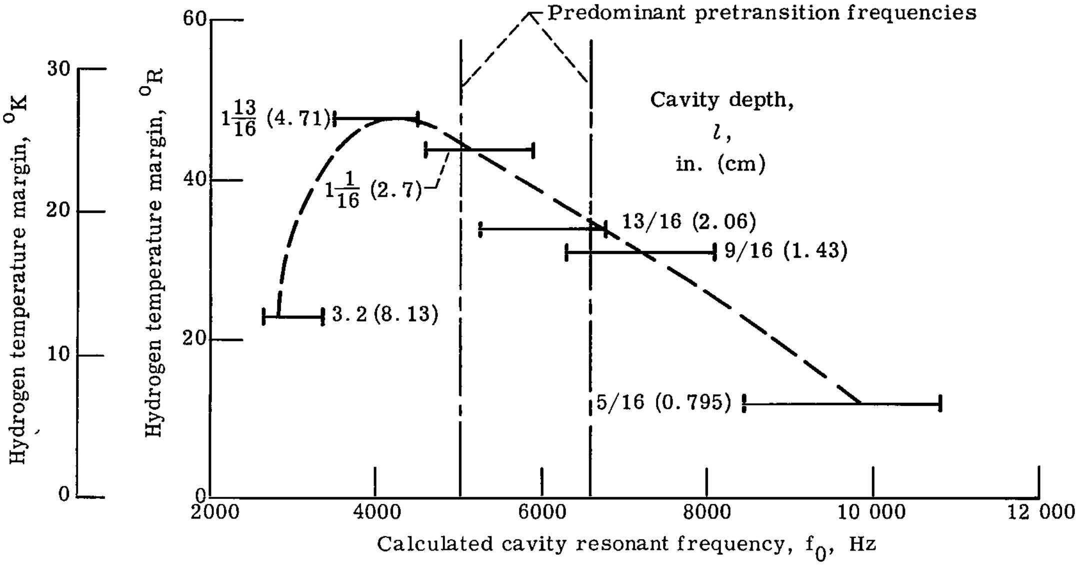

Figure 18. - Tuning curve for eight-row liner with injector I. Mixture ratio, 5. Data spread due to temperature variation.

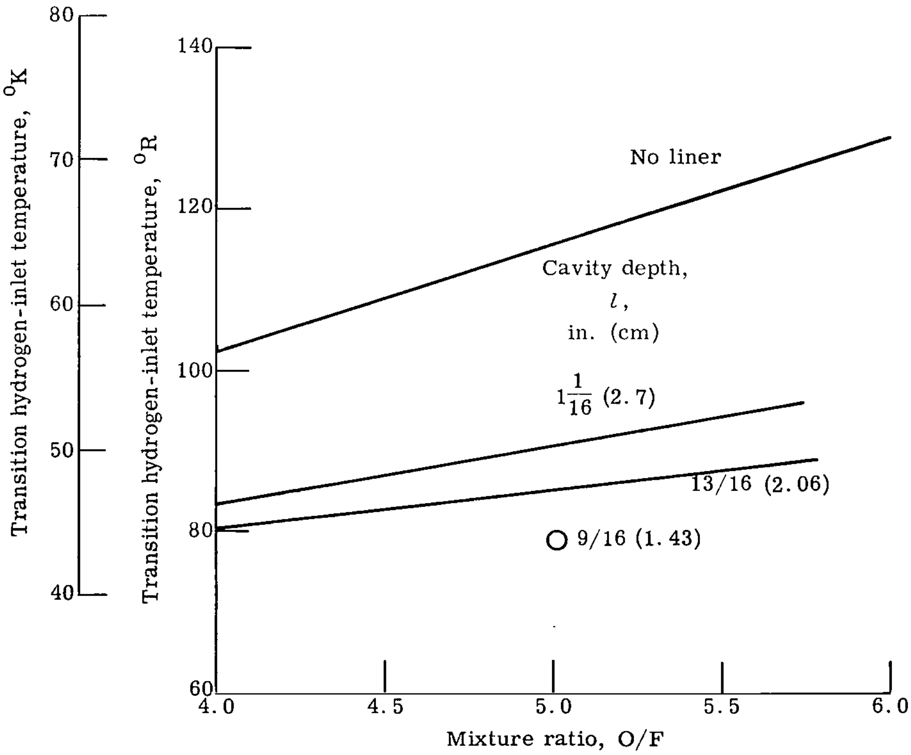

Figure 19. - Stability of partial-length liners (first row only) tested with injector I.

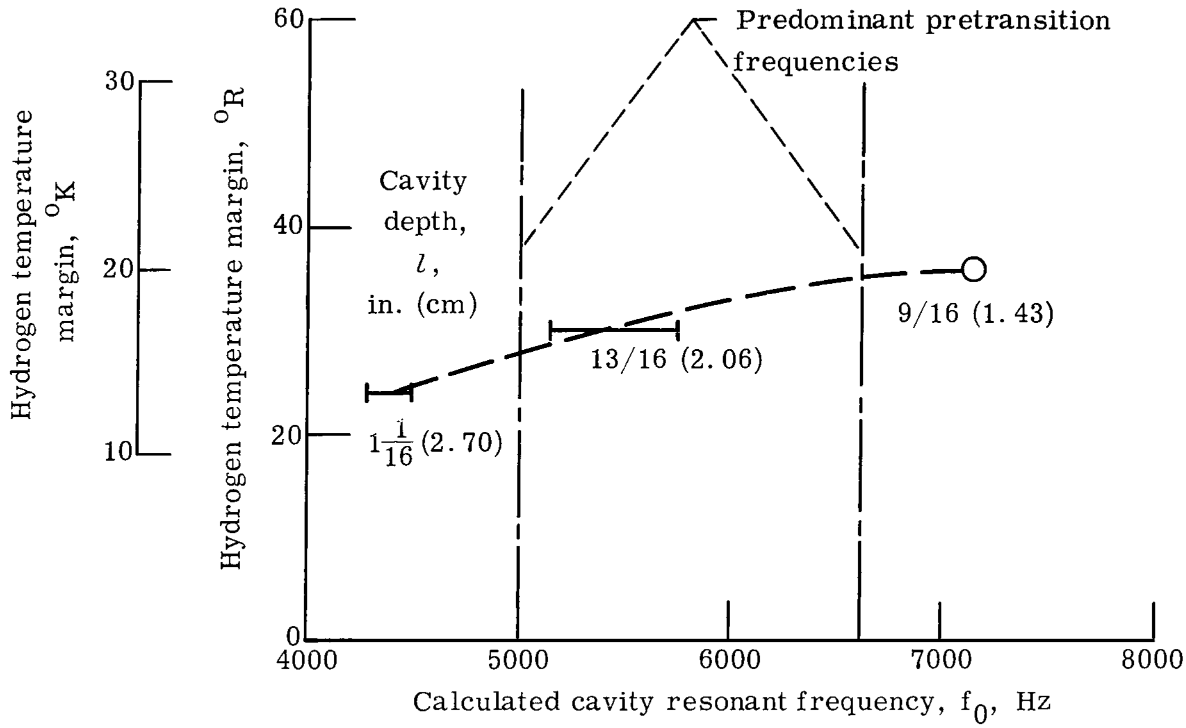

Figure 20. - Determination of design frequency for injector I. Calculated resonant frequencies for first row only. Mixture ratio, 5.

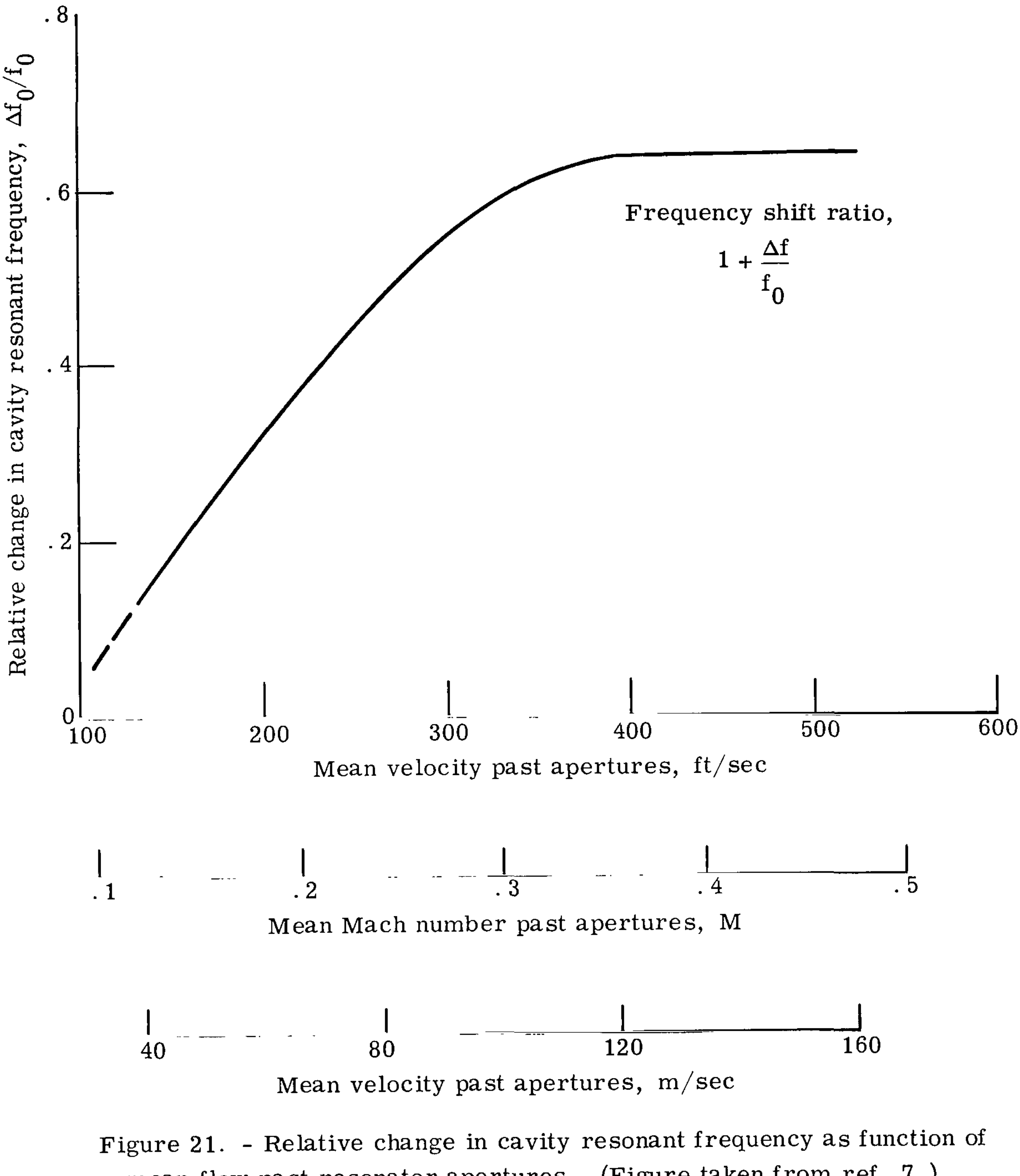

Figure 21. - Relative change in cavity resonant frequency as function of mean flow past resonator apertures. (Figure taken from ref. 7.)

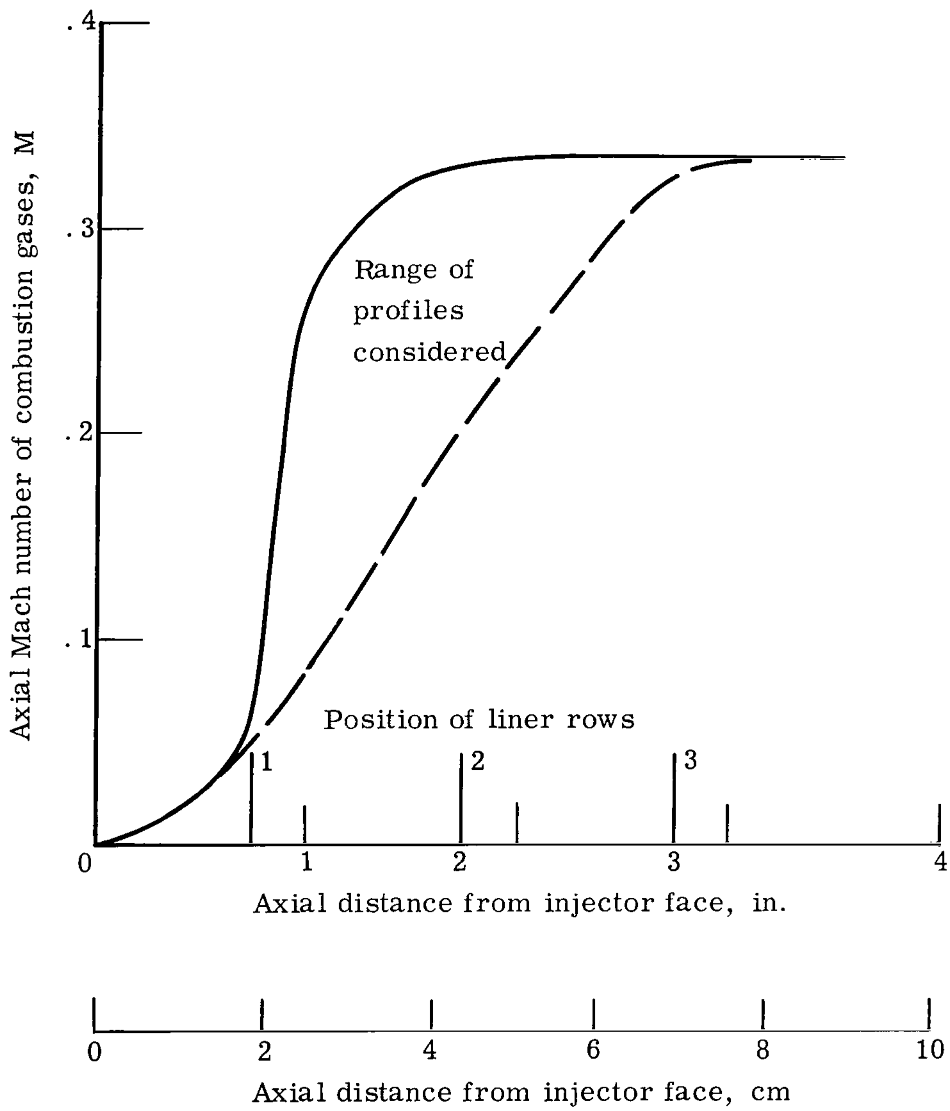

Figure 22. - Theoretical axial Mach number profiles (ref. 8). Mixture ratio, 5; chamber pressure, 300 psia (20.65×10^5 N/m^2).

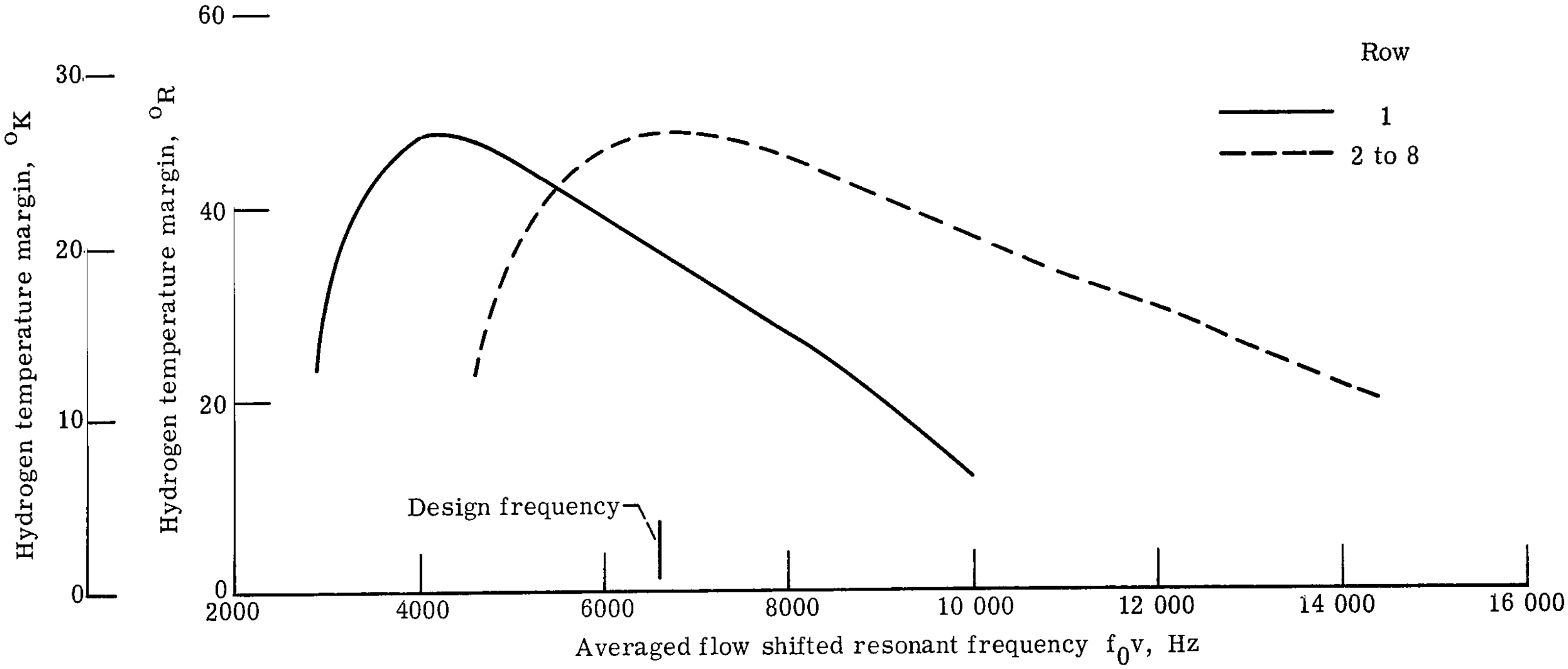

Figure 23. - Results of applying flow shifting to eight-row liner of injector I. Mixture ratio, 5.

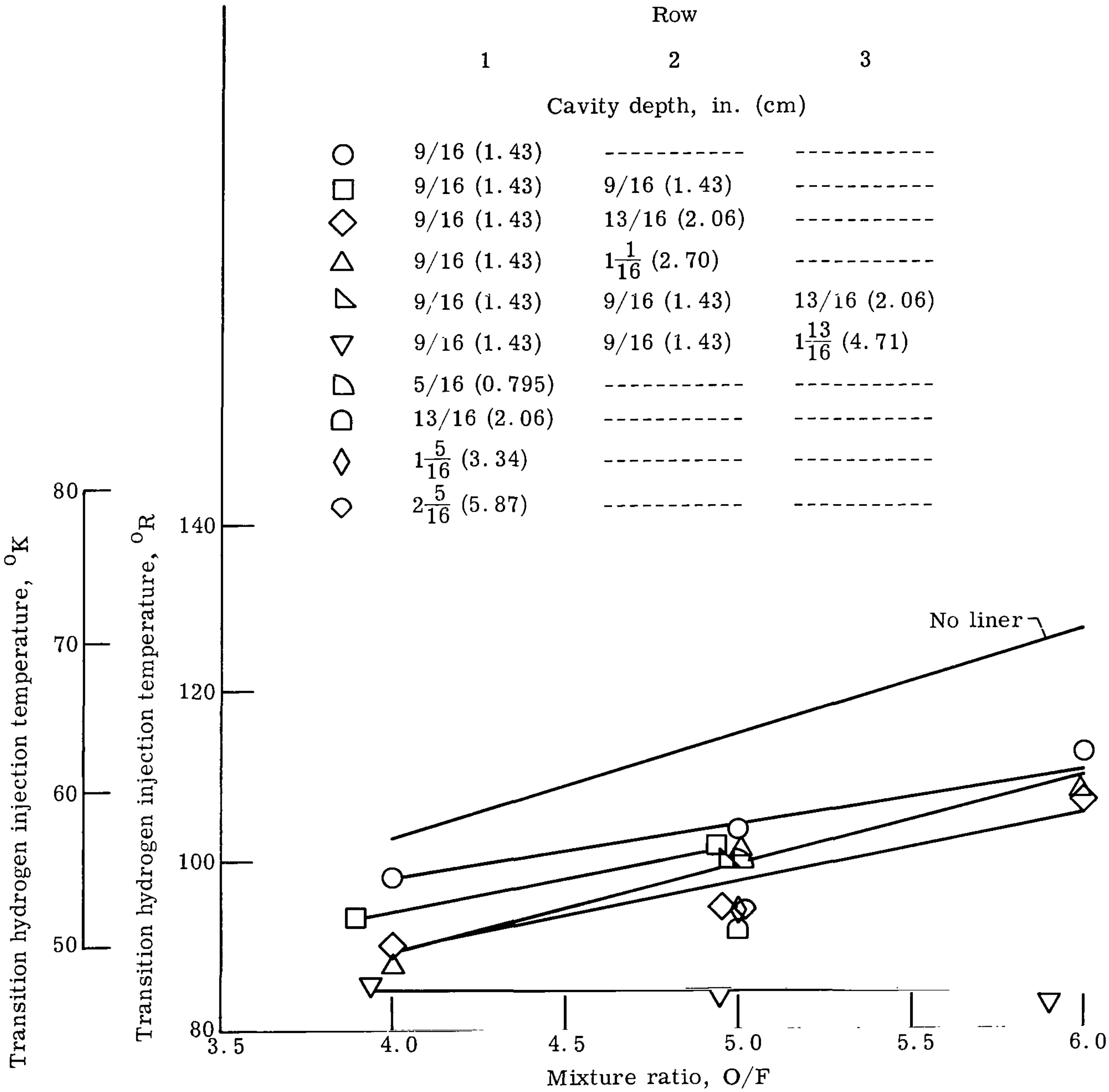

Figure 24. - Hydrogen temperature stability rating of partial-length liners with injector IIa.

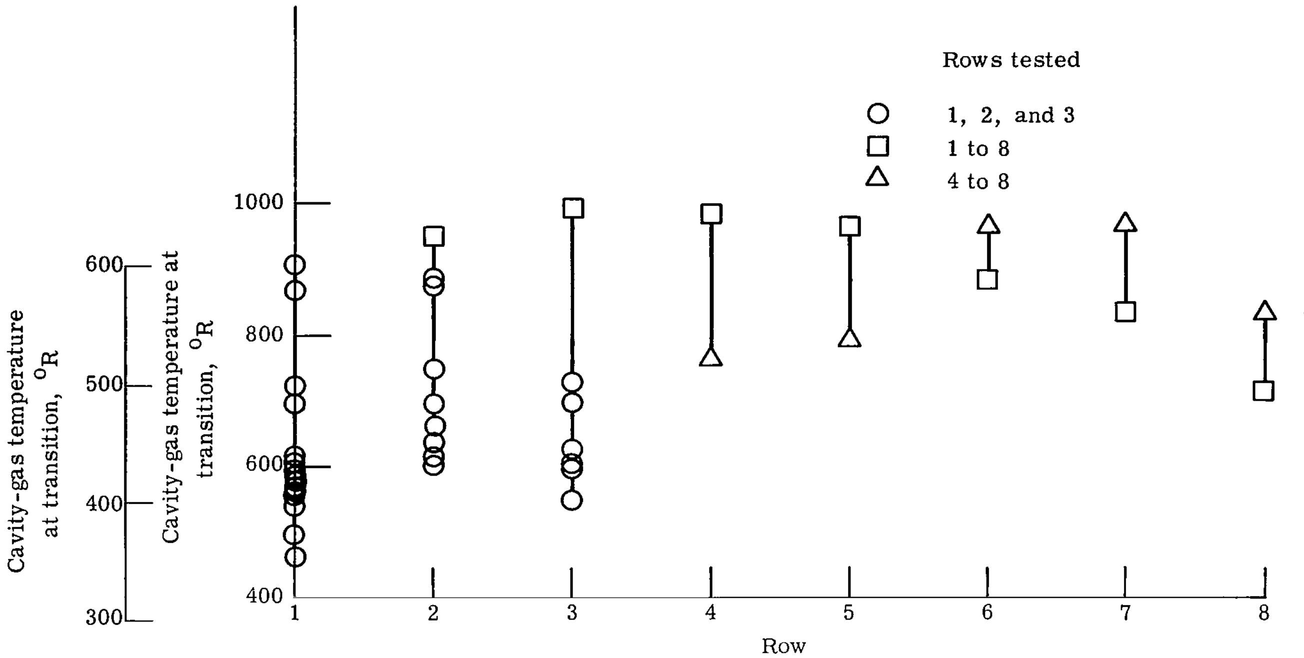

Figure 25. - Axial variation of cavity-gas temperature at transition for injector IIa. Mixture ratio for all configurations, 5.

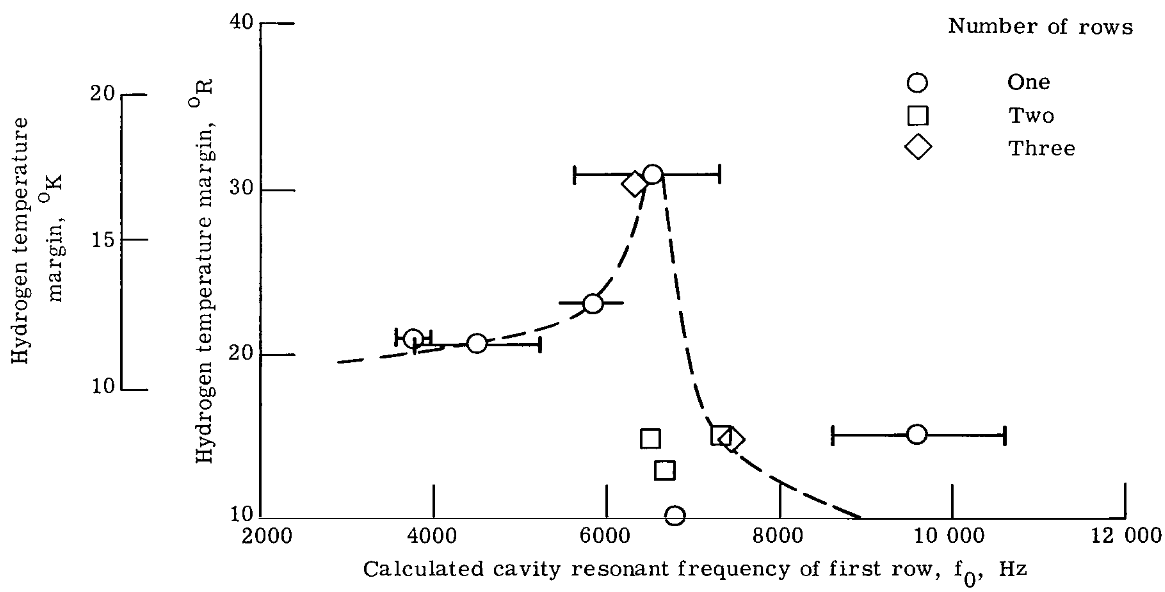

Figure 26. - Effect of liner length on stability of injector IIa. Mixture ratio 5. Plotted data are from table III.

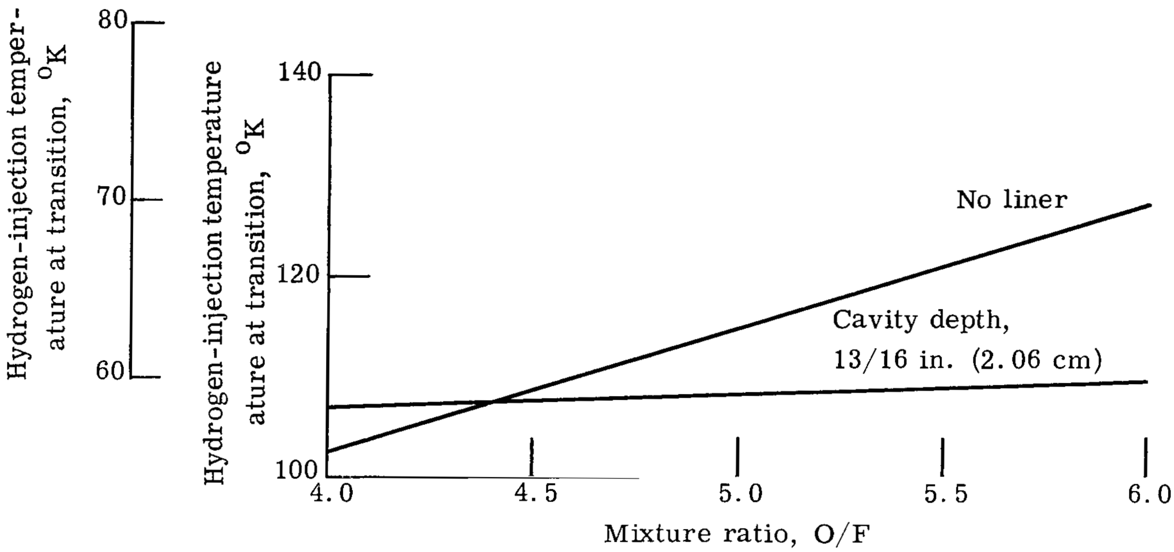

Figure 27. - Comparison of partial-length liners for rows 4 to 8. Injector IIa.

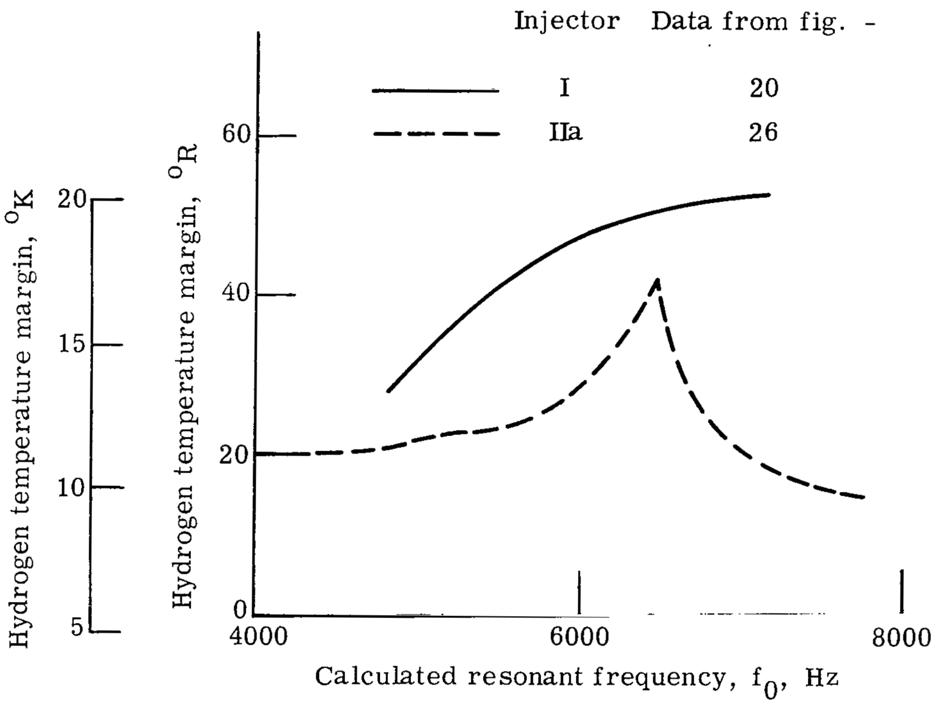

Figure 28. - Effect of injector on liner damping, composites of first-row liner results. Injectors I and IIa; mixture ratio, 5.

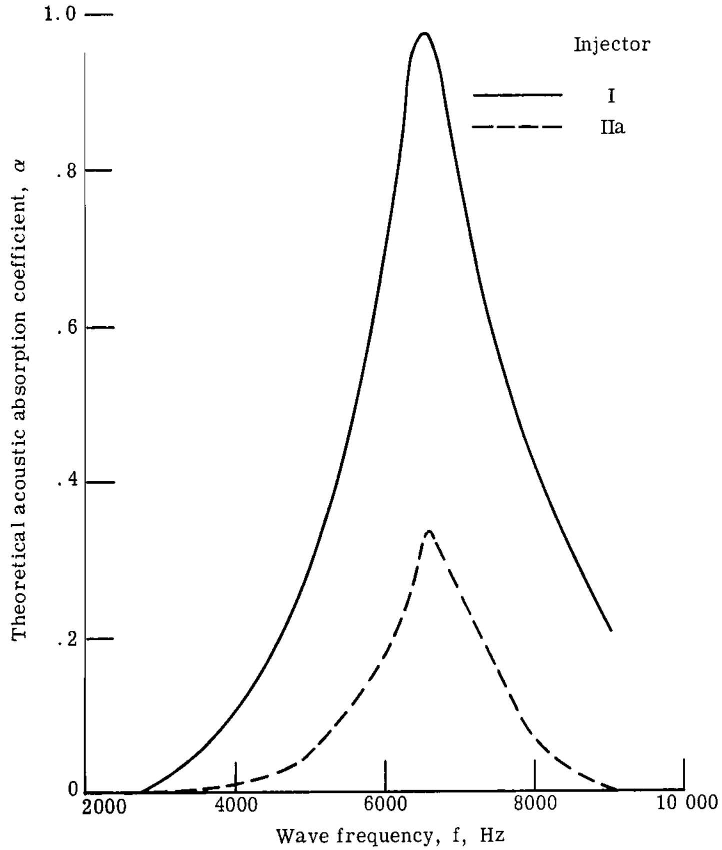

Figure 29. - Theoretical acoustic absorption coefficient as a function of wave frequency for injectors I and IIa.

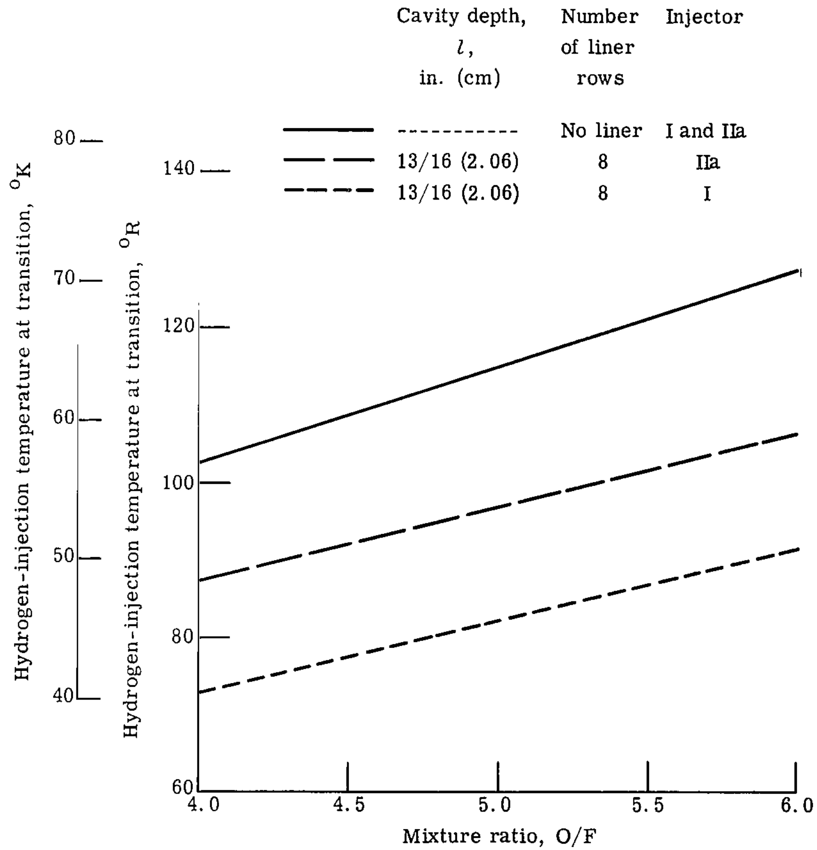

Figure 30. - Effect of injector on stability.

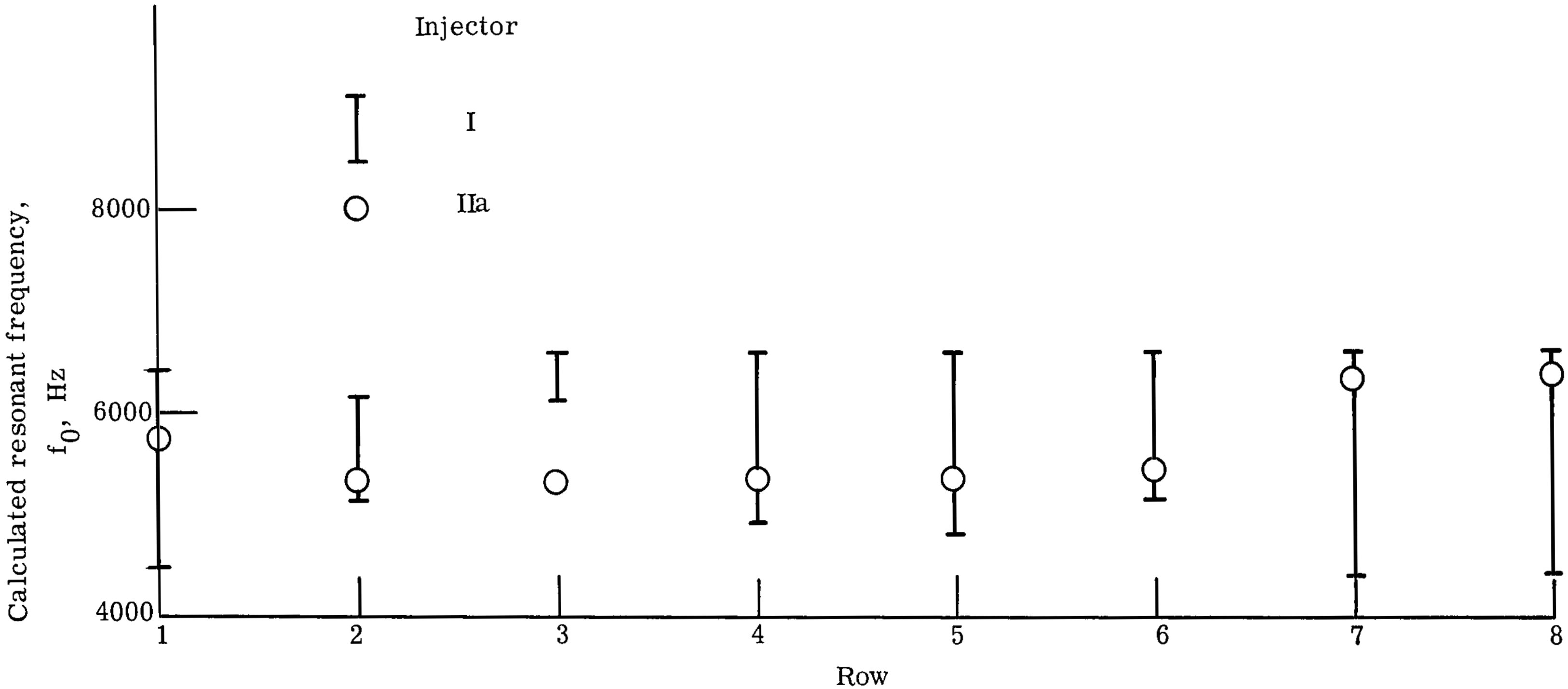

Figure 31. - Comparison of axial variation of calculated resonant frequency for eight-row liner with injectors I and IIa. Mixture ratio, 5.

National Aeronautics and Space Administration
WASHINGTON, D. C.

OFFICIAL BUSINESS

FIRST CLASS MAIL

POSTAGE AND FEES PAID
NATIONAL AERONAUTICS AND
SPACE ADMINISTRATION

04U 001 58 51 3DS 68074 00903
AIR FORCE WEAPONS LABORATORY/AFWL/
KIRTLAND AIR FORCE BASE, NEW MEXICO 87117

ATT MISS MADELINE F. CANOVA, CHIEF TECHNI
LIBRARY /WLIL/

POSTMASTER: If Undeliverable (Section 158 Postal Manual) Do Not Return

"The aeronautical and space activities of the United States shall be conducted so as to contribute . . . to the expansion of human knowledge of phenomena in the atmosphere and space. The Administration shall provide for the widest practicable and appropriate dissemination of information concerning its activities and the results thereof."

—NATIONAL AERONAUTICS AND SPACE ACT OF 1958

NASA SCIENTIFIC AND TECHNICAL PUBLICATIONS

TECHNICAL REPORTS: Scientific and technical information considered important, complete, and a lasting contribution to existing knowledge.

TECHNICAL NOTES: Information less broad in scope but nevertheless of importance as a contribution to existing knowledge.

TECHNICAL MEMORANDUMS: Information receiving limited distribution because of preliminary data, security classification, or other reasons.

CONTRACTOR REPORTS: Scientific and technical information generated under a NASA contract or grant and considered an important contribution to existing knowledge.

TECHNICAL TRANSLATIONS: Information published in a foreign language considered to merit NASA distribution in English.

SPECIAL PUBLICATIONS: Information derived from or of value to NASA activities. Publications include conference proceedings, monographs, data compilations, handbooks, sourcebooks, and special bibliographies.

TECHNOLOGY UTILIZATION PUBLICATIONS: Information on technology used by NASA that may be of particular interest in commercial and other non-aerospace applications. Publications include Tech Briefs, Technology Utilization Reports and Notes, and Technology Surveys.

Details on the availability of these publications may be obtained from:

SCIENTIFIC AND TECHNICAL INFORMATION DIVISION

NATIONAL AERONAUTICS AND SPACE ADMINISTRATION

Washington, D.C. 20546